HHS Public Access

Author manuscript

Sci Immunol. Author manuscript; available in PMC 2018 December 15.

Published in final edited form as:

Sci Immunol. 2018 June 15; 3(24): . doi:10.1126/sciimmunol.aat4956.

A recessive form of Hyper IgE Syndrome by disruption of ZNF341-dependent STAT3 transcription and activity

A full list of authors and affiliations appears at the end of the article.

[#] These authors contributed equally to this work.

Abstract

Heterozygosity for human *STAT3* dominant-negative (DN) mutations underlies an autosomal dominant form of hyper-IgE syndrome (HIES). We describe patients with an autosomal recessive form of HIES due to loss-of-function mutations of a previously uncharacterized gene, *ZNF341*. ZNF341 is a transcription factor that resides in the nucleus, where it binds a specific DNA motif present in various genes, including, most notably the *STAT3* promoter. The patients' cells have low basal levels of STAT3 mRNA and protein. The auto-induction of STAT3 production, activation, and function by STAT3-activating cytokines is particularly strongly impaired. Like patients with *STAT3* DN mutations, ZNF341-deficient patients lack Th17 cells, have an excess of Th2 cells, and low memory B cells, due to the tight dependence of STAT3 activity on ZNF341 in lymphocytes. Their milder extra-hematopoietic manifestations and stronger inflammatory responses reflect the lower ZNF341-dependence of STAT3 activity in other cell types. Human ZNF341 is essential for the *STAT3* transcription-dependent auto-induction and sustained activity of STAT3.

One Sentence Summary:

ZNF341 is a newly characterized transcription factor controlling baseline and inducible transcription of the human *STAT3* gene.

Introduction

Hyper-immunoglobulin (Ig)E Syndrome (HIES) is a relatively common primary immunodeficiency (PID) (OMIM #147060), first described as Job's Syndrome by Wedgwood in 1966, and renamed HIES by Buckley in 1972 (1, 2). It was subsequently

[*]Correspondence: anne.puel@inserm.fr (A.P.), jean-laurent.casanova@rockefeller.edu (J.L.C), vivien.beziat@inserm.fr (V.B.).

Author Contributions

V.B., A.P., and J.-L.C. designed the study and wrote the manuscript. V.B., J.L., C.S.M., Y.W., Y.Z., R.L., T.L., A.I.L., G.R., K.P., S.J.P, D.T.A., E.K.D., B.P., R.G., A.G., M.M., M.T. performed the experiments. F.A., J.C., A.B., V.R., M.B., H.T., D.C., N.M. conducted exome, linkage, microarray, and statistical analyses. A.B., I.P., S.Z., S.B., S.K., P.G., F.A., I.B., J.E.B., O.W., I.M.F., B.F., M.O.C., S.F., M.A.A., M.L.V., C.P., A.H., A.S., A.O., N.R., T.C., provided material from the patients and reagents. J.X.L., P.L., N.D and W.J.L. performed and analyzed the ChIP-seq. B.G., J.C.B., B.B., I.M., J.P.D.S, L.A., S.G.T. provided expertise and feedback. J.-L.C., A.P., and V.B. secured funding. All the authors critically reviewed the manuscript.

Competing Interests

The authors have no conflicts of interest to declare.

Data and Materials Availability

The RNA-seq and ChIP-seq data are available on GEO under the deposit number GSE113194. The microarray data are available on GEO under the deposit number GSE113889 and GSE113945, respectively.

shown to typically display autosomal dominant (AD) inheritance, with variable expressivity (3). AD-HIES is characterized by bacterial infections, including, in particular, various staphylococcal diseases, and fungal infections, such as chronic mucocutaneous candidiasis (CMC) in particular. In the course of infection, clinical and biological signs of inflammation are paradoxically weak in these patients. Patients also display cutaneous and systemic manifestations of allergy (in the broad sense of the term), along with high serum concentrations of total and allergen-specific IgE, and extrahematopoietic features, including facial dysmorphia, deciduous tooth retention, osteopenia, hyperextensibility, and vascular abnormalities (3, 4). They also have B-cell and Ab deficiencies (5). In 2007, Minegishi identified heterozygous, dominant-negative (DN) mutations of the gene encoding STAT3 as responsible for AD-HIES (6). Most, if not all cases of AD-HIES are caused by *STAT3* DN mutations (7–9).

Some non-hematopoietic features of AD-HIES were explained by the discovery of patients with overlapping phenotypes, carrying biallelic mutations of genes encoding leukemia inhibitory factor receptor (LIFR), IL-11R, and the IL-6ST/gp130 common subunit of the IL-6 receptor family, which signal via STAT3 in various extrahematopoietic cells (10–12). Myeloid cell development is essentially normal in AD-HIES, but lymphocyte development is severely affected, with low frequencies of $CD4^+$ and $CD8^+$ central memory T cells, Th17 cells, Tfh cells, MAIT cells, NKT cells, and memory B cells (5, 7, 13–17). Patients with inborn errors of receptors or cytokines upstream from STAT3 display overlapping syndromes. Indeed, memory B-cell deficiency has been detected in IL-6ST-deficient patients and in IL-21R-deficient patients, who also have low frequencies of central memory $CD8^+$ T cells, Tfh cells, and NKT cells (15, 18, 13, 19, 17, 12).

Some leukocyte functions are also abnormal in AD-HIES patients, as shown by studies *in vitro*. The patients' naïve $CD4^+$ T cells display impaired Th17 differentiation upon stimulation under Th17-polarizing conditions *in vitro*, providing a mechanism for the patients' CMC, as seen in patients with inborn errors of IL-17 immunity (14, 20, 21). $CD4^+$ T cells are also biased toward the Th2 lineage, accounting for some of the patients' allergic manifestations (22), whereas the inability of their naïve B cells to differentiate into plasma cells upon stimulation with CD40L and IL-21 underlies Ab deficiency, which is also observed in patients with mutations of *IL21* or *IL21R* (5, 18, 19). Finally, IL-10 does not inhibit the response of the patients' myeloid cells to LPS (6, 23). Nevertheless, these patients do not display the early-onset colitis observed in patients with IL-10, IL-10R1, and IL-10R2 deficiencies (24). Finally, poor responses of myeloid cells to IL-6 and related cytokines probably account for the patients' low levels of inflammation, as inferred from the patient with IL-6ST deficiency (12).

In this context, we investigated patients with an autosomal recessive (AR) form of HIES, including CMC, staphylococcal infections, severe allergy and high serum IgE levels, but apparently with stronger inflammatory responses and fewer extrahematopoietic manifestations than patients with AD-HIES. Their phenotype was more closely resembled that of patients with *STAT3* DN mutations than that of patients with other PIDs involving high serum IgE levels often referred to as AR forms of HIES, such as DOCK8 deficiency (25–29) and PGM3 deficiency (30, 31). Indeed, patients with DOCK8 deficiency present

none of the extrahematopoietic features of AD-HIES but are highly vulnerable to skin-tropic viral infections. Likewise, patients with PGM3 deficiency display different extrahematopoietic manifestations, auto-immunity, and a broader susceptibility to infections. We thus tested the hypothesis that the patients studied suffered from a previously undescribed AR inborn error of immunity, closely related to the AD form of HIES. Given the clinical similarity of the AD and AR forms of HIES, we hypothesized that the disease-causing gene underlying the AR form would encode a protein physiologically related to STAT3.

Results

The patients are homozygous for truncating mutations of *ZNF341*

We investigated eight patients from six unrelated families, of Moroccan (kindred A), Afro-Caribbean (kindred B), Iranian (kindred C), Turkish (kindreds D, E), and Lebanese (kindred F) descent (Fig. 1A-B, Fig. S1A-J, Table S1–2 and case reports). Four families were known to be consanguineous, whereas the other two families were shown to be consanguineous by whole-exome sequencing (WES), which revealed a high percentage of homozygosity in the patients (32) (Fig. S1K). We performed genome-wide linkage (GWL) analysis on the three living patients from kindreds A and B (P2, P3, and P4), testing the hypothesis of a shared AR trait with full penetrance (Fig. S1L-M). A single 16.8 Mb region on chromosome 20 provided a significant cumulative LOD score of 4.8 (Fig. S1M). We also performed WES for these three patients (Fig. S1N). Within the linked region containing 162 protein-coding genes, only *ZNF341*, a gene of unknown function, displayed homozygosity for a rare variant (Table S3). This variant (*c.904C>T*) was the same in both families tested, and caused replacement of the arginine 302 codon with a premature stop codon (R302X). By WES (P5, P6, and P7) and Sanger sequencing (P8), we showed that the other four unrelated patients from kindreds C-F also carried homozygous mutations of *ZNF341*. Kindred C displayed the same *c.904C>T* mutation (R302X), whereas kindred D had a frameshift deletion (*c.1062delG*) leading to a premature stop codon (K355fs), kindred E had a nonsense mutation (*c.1626C>G*) replacing the tyrosine 542 codon with a premature stop codon (Y542X), and kindred F had a nonsense mutation (*c.583C>T*) replacing the glutamine 195 codon with a premature stop codon (Q195X). Sanger sequencing confirmed all the mutations identified by WES. The segregation of the four mutant alleles of *ZNF341* in the six families was consistent with a fully penetrant AR trait (Fig. 1A and Fig. S1O-T). The K355fs, Y542X, and Q195X mutations were private to kindreds D, E, and F, respectively. There were only two R302X heterozygotes in the ExAC database. Kindreds A, B, and C, which carried R302X, belonged to three different ethnic groups, as confirmed by principal component analysis (Fig. S1U) (32). The mutation was recurrent due to a hotspot rather than a founder effect, as the haplotypes encompassing *ZNF341* differed between the three families (Fig. 1C). The four *ZNF341* mutations are located in four different exons, scattered across the gene. They are the only known mutations of this gene predicted to be loss-of-function and found in the homozygous state in public and in-house databases. Moreover, these mutations also have the four highest damage prediction scores (CADD, combined annotation dependent depletion) of all the variants found to be homozygous (Fig. 1D) (33, 34).

Together, these findings strongly suggest that the homozygous *ZNF341* mutations identified in these patients are both deleterious and disease-causing.

The mutant *ZNF341* alleles do not encode full-length isoforms

Nothing is known about the biology of *ZNF341*. The human gene has 15 exons and encodes two main transcripts, differing by 21 in-frame nucleotides due to alternative splicing involving different acceptor sites at the 3' end of exon 6 (Fig. 1E), and yielding proteins of 847 (isoform 1) or 854 (isoform 2) amino acids. The stop codons created by Q195X and R302X are upstream from these 21 nucleotides, unlike those created by K355fs and Y542X. The encoded protein has 12 predicted DNA-binding C2H2 zinc finger (ZNF) domains, and two predicted nuclear localization sequences (NLS), suggesting it is a transcription factor (Fig. 1E) (35, 36). The stop codons created by Q195X and R302X are upstream from the two NLS, whereas those created by K355fs and Y542X are located between them. We transfected HEK293T cells with cDNAs encoding wild-type (WT) ZNF341 (isoforms 1 and 2), Q195X or R302X (both of which encode a single isoform), K355fs (isoform 1), K362fs (isoform 2), Y542X (isoform 1), or Y549X (isoform 2), and analyzed the products by western blotting with a polyclonal Ab (pAb) against the N-terminal segment of ZNF341 (HPA024607) (Fig. 2A and Fig. S2A). Isoforms encoded by the WT (predicted MWs of ~92 and 93 kDa), K355fs/K362fs (~40 and ~41 kDa), and Y542X/Y549X (~58 and ~59 kDa) cDNAs were detected in the nucleus, whereas those encoded by the Q195X (~20 kDa) and R302X (~31 kDa) cDNAs were retained in the cytoplasm. We transfected SV40-transformed fibroblasts from P4 (R302X/R302X) with cDNAs encoding C-terminally V5-tagged proteins. We then analyzed the subcellular distribution of these proteins by confocal microscopy with a V5-specific monoclonal Ab (mAb) (Fig. 2B and Fig. S2B). Both isoforms of the WT, and the K355fs, K362fs, Y542X, and Y549X proteins were localized in the nucleus, whereas the R302X (and by inference R195X) proteins were retained in the cytoplasm. We co-expressed cDNAs encoding WT isoform 1, WT isoform 2, R302X, K355fs, and Y542X, each tagged with V5 or DDK, in HEK293T cells. Immunoprecipitation and immunoblotting suggested that both WT ZNF341 isoforms could homo- or hetero-oligomerize (Fig. 2C). Homo- and hetero-oligomerization of the mutant proteins were impaired, but not abolished (Fig. S2C, D). In this system, we detected no interaction between WT ZNF341 and STAT3, even upon stimulation (Fig. S2E). Thus, none of the four mutant alleles encodes a full-length ZNF341 isoform; their products are truncated and oligomerize poorly, and two of the mutant proteins (Q195X and R302X) are retained in the cytoplasm.

Full-length ZNF341 isoforms are not detected in the patients' cells

Public databases suggest that *ZNF341* is ubiquitously transcribed (FANTOM5, HPA, and GTEx). We studied the expression of endogenous *ZNF341* in cell lines from healthy controls and patients. PCR and sequencing showed that both full-length transcripts were present in Epstein-Barr virus (EBV)-transformed B cells from P4 (Fig. S2F-I), and in herpes virus Saimiri (HVS)-transformed T cells from P3 and P4 (Fig. S2J). Moreover, total *ZNF341* mRNA levels, as determined by RT-qPCR, were significantly higher in EBV-B cells and slightly higher in HVS-T cells from all patients tested (P3, P4, P6, P7) than in controls, suggesting that these mutations did not provoke nonsense-mediated mRNA decay in these

cells, and that WT ZNF341 downregulates its own transcription (Fig. 2D, E). We also detected *ZNF341* mRNA in primary human umbilical vein endothelial cells (HUVECs), three hematopoietic and nine non-hematopoietic cancer cell lines tested, and in control SV40-transformed fibroblasts and primary keratinocytes (Fig. S2K-M). We performed western blotting with a ZNF341-specific pAb (HPA067108), or an in-house mAb (8B3.1), both raised against C-terminal residues 366–468 (downstream from G195, R302, and K355 but upstream from Y542 in isoform 1). We detected ZNF341 (~100 kDa) in the nuclei of all nine cancer cell lines, in primary HUVECs, primary and SV40-transformed fibroblasts, and primary keratinocytes from healthy donors (Fig. S2N-P). By contrast, ZNF341 was not detected in primary and SV40 fibroblasts or in keratinocytes from P2, P3, and P4 (Fig. S2O, P). Similarly, we detected full-length ZNF341 (~100 kDa) in the nuclei of six hematopoietic cell lines (RAJI, Jurkat, K562, U937, HL-60 and clone 15 HL-60) (Fig. S2N), and EBV-B and HVS-T cells from healthy controls, but not any of the four patients tested (corresponding to three mutations) (Fig. 2F, G). A protein of lower MW (~70 kDa) was observed in the nuclei of EBV-B cells from P7, whose Y542X mutation is predicted to preserve the 8B3.1 mAb epitope (Fig. 2F). As the pAb (HPA024607) recognizing the N-terminal segment failed to detect endogenous ZNF341 in control cells, we cannot exclude the possibility that low levels of the truncated R302X (and Q195X) and K355fs proteins were also present in the cytoplasm and nucleus, respectively, of the corresponding patients' cells. Finally, production of the full-length ZNF341 protein was rescued in the EBV-B cells of P4 (R302X) and HVS-T cells of P3 (R302X) by stable transduction with WT *ZNF341* (isoform 1) (Fig. 2F, G). Together, these data indicate that both full-length ZNF341 isoforms are absent from the nuclei of primary keratinocytes, primary and SV40-fibroblasts, EBV-B, and HVS-T cells derived from patients with various mutations of *ZNF341.*

ZNF341 deficiency alters the development of lymphoid, but not myeloid subsets

We analyzed the pattern of *ZNF341* expression in leukocyte subsets from healthy controls. *ZNF341* transcripts for both isoforms were detected, in similar amounts, in monocytes, NK, B, $CD4^+$, and $CD8^+$ T cells, by RT-qPCR and RT-PCR (Fig. 2H and Fig. S2Q). Accordingly, a single protein corresponding to either or both isoforms was detected in the nucleus of T, B, NK, monocytes (including both $CD14^+$ and $CD16^+$ subsets), basophils, and dendritic cells (including PDCs, cDC1, and cDC2) (Fig. 2I-L). ZNF341 was also detected in the HL-60 and clone 15 HL-60 cell lines (Fig. S2N), two acute promyelocytic leukemia cell lines. These lines can be differentiated into neutrophil-like and eosinophil-like cells *in vitro* respectively, suggesting that primary neutrophils and eosinophils may express ZNF341, like basophils (Fig. 2L). In this context, we analyzed the distribution of leukocyte subsets in the patients, by flow cytometry. The seven patients tested (P2–P8) had normal counts of circulating neutrophils and basophils, monocytes, B and T cells, but low counts of NK cells (Table S2, case reports). Eosinophil counts were high in three patients (Table S2, case reports). The proportions of myeloid (cDC1, cDC2) and plasmacytoid (pDC) dendritic cells (Fig. S3A), and of monocyte subsets (Fig. S3B) were normal. $CD56^{bright}$ NK cells were more abundant among NK cells, but their maturation profile was otherwise normal (Fig. 3A). The proportions of ILCs among peripheral blood mononuclear cells (PBMCs) were also low, particularly for ILC1 and ILC2 (Fig. 3B). The global proportion of circulating memory B cells was low (Fig. 3C), with low (IgM^+, IgA^+) and high (IgG^+) proportions of Ig isotype-

specific memory B cells (Fig. 3D), consistent with the patients' high serum concentrations of IgG1 and IgG4 (Table S2). The patients had normal or subnormal serum titers of antigen-specific Abs after infection with common pathogens (Table S2) and P4 displayed a normal response to a vaccine booster injection (Table S2). The patients' T cells proliferated normally in response to mitogens and antigens *in vitro* (Table S2). The patients had a higher proportion of naive $CD4^+$ T cells, and lower proportions of central memory $CD4^+$ and $CD8^+$ T cells, and of MAIT cells, than controls, but normal proportions of Treg, γδ-T cells, and iNKT cells (Fig. 3E-G). Strikingly, this distribution of leukocyte subsets very closely resembles that of patients with HIES due to *STAT3* DN mutations, who also have high frequencies of naïve $CD4^+$ T cells and low frequencies of $CD4^+$ and $CD8^+$ central memory T cells, memory B cells, MAIT cells (5, 7, 13, 15–17), and ILC1 and ILC2 cells (Fig. 3B). However, ZNF341-deficient patients also have low NK cell counts (Table S2, Fig. 3A).

ZNF341 is a transcription factor that binds the *STAT3* promoter in T and B cells

We performed ChIP-Seq analysis with the anti-ZNF341 mAb 8B3.1, to determine whether ZNF341 bound DNA *in vivo* and to identify its binding sites throughout the genome. In EBV-B cells from P4 transduced with cDNAs encoding WT ZNF341 isoforms 1 and 2, we found 5,842 and 6,570 ZNF341-binding DNA regions, respectively, 5,003 of which were common to both isoforms. We also analyzed healthy control T cells activated with plate-bound anti-CD3 and soluble anti-CD28 antibodies: we identified 1,457 binding regions, only 229 of which were common to EBV-B cells. Computational analysis revealed two top-ranked motifs, a ZNF-like binding motif GGAAC/GA/GGC ($p = 5\times10^{-437}$) and an Sp1-like binding motif GGGAGG ($p = 3.7\times10^{-44}$) (Fig. 4A). The ZNF-like and Sp1-like motifs have not been described before, and the closest known motifs, for ZNF263 and Sp1, respectively, are markedly different (Fig. S4A, B). The strongest ZNF341-binding site in both EBV-B cells and T cells was located in the *STAT3* promoter ($p = 10^{-310}$ being the most significant *p*-value of all binding sites). Strong ZNF341 binding was also observed for the *STAT1* promoter and *ZNF341* intron 1 ($p = 10^{-242}$ and 10^{-310}, respectively) (Fig. 4B). Furthermore, in the 229 motifs common to both control T cells and patient EBV-B cells transduced with ZNF341, we also identified bipartite binding sites containing the Sp1-like motif GGGAGG upstream from the ZNF-like motif GGAAC/GA/GGC ($p < 5.3\times10^{-172}$) (Fig. 4A). We found that there was a preferential spacing of 13 to 14 nucleotides between the two motifs (Fig. 4C, D), associated with a stronger binding intensity, as assessed by determining peak intensity (Fig. S4C). We then incubated nuclear extracts of HEK293T cells transfected with an empty vector, the C-terminal DDK-tagged WT, R302X, K355fs, or Y542X *ZNF341* cDNA with a 5'-tagged fluorescent DNA probe containing the putative bipartite ZNF341-binding motif from the *STAT3* promoter (Fig. 4E and Fig. S4D). In electrophoretic mobility shift assays (EMSAs), nuclear proteins from WT-transfected cells bound the probe, whereas complex formation was inhibited by an unlabeled specific probe (CP), and super-shifting of the complex was observed with the specific anti-ZNF341 8B3.1 or anti-DDK mAb but not with an isotype control mAb. By contrast, nuclear proteins from R302X- and K355fs-transfected cells did not bind the probe, whereas Y542X-transfected cells displayed weak binding (Fig. 4E and Fig. S4D). Incubation of the same nuclear extracts with a 5' biotinylated DNA probe resulted in the pulldown, with streptavidin-coupled magnetic beads, of complexes consistent with the EMSA results (Fig. 4F). Pulldown experiments with

nuclear extracts from healthy control resting primary $CD3^+$ T cells or EBV-B cells showed that endogenous WT ZNF341 bound efficiently to the bipartite DNA binding motif (Fig. 4G, H). By contrast, the truncated Y542X ZNF341 protein was not pulled down in this system, in experiments with nuclear extracts from P7 EBV-B cells (Fig. 4H). Thus, WT ZNF341 specifically binds a bipartite consensus DNA motif that is present in the promoter of *STAT3*, whereas the three mutant ZNF341 proteins tested (and, by inference, Q195X), including K355fs and Y542X, which can translocate to the nucleus, do not.

ZNF-like and Sp1-like motifs cooperate to enhance ZNF341 DNA binding

We characterized the ZNF341-binding motif in more detail, by testing WT ZNF341 in pulldown experiments with probes either corresponding to the bipartite DNA binding motif or containing various systematic mutations (Fig. S4E, F). We deleted the Sp1-like (ΔSp1 probe) or the ZNF-like (ΔZNF probe) motif, or introduced single-nucleotide (n=8; probes #1 to #8) or multiple-nucleotide mutations (n=4; #4#7, aA, aG, and aZ probes) at various positions in the ZNF-like motif. Nuclear extracts from HEK293T cells transfected with WT ZNF341 isoform 1 cDNA or an empty vector were used as positive and negative controls, respectively. The deletion of the Sp1-like (74%) or ZNF-like (94%) motif decreased ZNF341 binding relative to the consensus sequence (WT probe), and deletion of the ZNF-like motif had the strongest impact (Fig. S4E). This result is consistent with our ChIP-seq data, showing that the ZNF-like motif is present in all 500 top peaks, whereas the Sp1-like motif is present in only 45% of these peaks. In a similar pulldown experiment, single-nucleotide mutagenesis of the ZNF-like motif (GGAACAGC) only modestly decreased ZNF341 binding relative to the WT consensus DNA sequence (Fig. S4F). However, mutations of one of the most (#3) and one of the least conserved nucleotides (#5) within the ZNF-like motif were associated with the largest (82%) and smallest (40%) decreases in DNA binding, respectively. Replacements of multiple nucleotides within the ZNF-like motif (aZ, aA and aG probes) decreased DNA binding by about 94%, to levels similar to those observed with a probe lacking the ZNF-like motif (ΔZNF probe). Overall, although either motif within the bipartite sequence is sufficient for at least some detectable binding of ZNF341 to DNA, the ZNF-like motif is more important and acts in synergy with the Sp1-like motif to ensure strong binding of ZNF341 to DNA.

ZNF341 overexpression drives the induction of *STAT3*

We assessed the ability of ZNF341 to induce transcription from the *STAT1* and *STAT3* promoters (44 bp of each promoter containing the canonical bipartite motif) in a luciferase reporter assay in HEK293T cells (Fig. 4I and Fig. S4G, H). Both WT isoforms induced expression from the *STAT1* and *STAT3* promoters. Three of the five mutant isoforms tested induced no luciferase activity, confirming that the R302X and K355fs/K362fs mutant alleles (and, by inference, Q195X) were loss-of-function. By contrast, the Y542X/Y549X mutant, which bound the canonical motif on EMSA and in pulldown experiments in the overexpression system, but not in EBV-B cells from P7, yielded intermediate levels of luciferase activity, suggesting that it is hypomorphic, at least when overexpressed. The luciferase *STAT1* and *STAT3* constructs containing the Sp1-like or the ZNF-like motif alone failed to induce luciferase activity in the presence of WT ZNF341, demonstrating the requirement of both motifs for ZNF341 activity (Fig. S4G, H). Cotransfection with the WT

ZNF341 cDNA together with a *Sp1* cDNA did not further enhance luciferase activity from *STAT3* or *STAT1* bipartite canonical sequences over that observed for WT *ZNF341* alone (Fig. S4I). Consistently, following the overexpression of Sp1 and ZNF341 in HEK293T cells, no interaction was detected between these two proteins in immunoprecipitation experiments (Fig. S4J). In conclusion, ZNF341 induces the transcription of *STAT1* and *STAT3* by binding to the bipartite consensus sites in their promoters. Two of the three mutant alleles tested are loss-of-function (R302X and K355fs), the third being at least severely hypomorphic (Y542X), and the fourth is predicted to be loss-of-function (Q195X). In light of the clinical and immunological similarities between patients with *ZNF341* and *STAT3* mutations, these findings strongly suggest that ZNF341 may be essential for the transcription of *STAT3*, at least in cells expressing ZNF341, the pattern of expression of which is apparently as broad as that of STAT3.

STAT3 function is normal in ZNF341-deficient immortalized cell lines

We performed total RNA sequencing (RNA-Seq), to determine whether ZNF341 controlled the transcription of target genes, including *STAT3* in particular, in immortalized lymphoid cell lines. *ZNF341* overexpression had very little impact on the transcriptome of P4 EBV-B cells (Fig. 4J). We found that, following transduction with WT ZNF341 isoform 1 or 2, mRNA levels differed significantly ($p<0.01$) from those in cells transduced with an empty vector for only 28 and 52 mRNAs (Tables S4, 5), respectively, including *STAT1* (fold-change, FC=3.0 and 3.3), but surprisingly not *STAT3* (FC=1.4 and 1.6) (Fig. 4K). Thus, the binding of ZNF341 to the promoters of *STAT3* and other genes does not strongly drive their transcription in EBV-B lines. We then analyzed STAT1 and STAT3 mRNA and protein levels in cell lines from patients and controls (Fig. 4SK-O). We found that *STAT1* mRNA levels were in the lower part of the control range in EBV-B cells, HVS-T cells, and in SV40-immortalized fibroblasts from patients, as determined by RT-qPCR (Fig. S4K). STAT1 protein levels were also lower (~2–3 fold) in the patients' EBV-B cells, HVS-T cells, and SV40-fibroblasts than in controls, as shown by western blotting and flow cytometry (Fig. S4L-O). The complementation of HVS-T cells from P3 and EBV-B cells from P4 with WT *ZNF341* increased STAT1 mRNA and protein levels, as shown by comparison with cells transduced with an empty vector (Fig. S4K-O). By contrast, STAT3 mRNA and protein levels were within or near the normal range in EBV-B cells from the patients (Fig. S4K, L, O). These levels were slightly lower in patient HVS-T cells and SV40-fibroblasts (Fig. S4K, M-O). The transduction of HVS-T cells from P3 and EBV-B cells from P4 with WT *ZNF341* increased STAT3 mRNA and protein levels relative to those in cells transduced with an empty vector (Fig. S4K-M, O). Finally, the amounts of phosphorylated STAT1 and STAT3 were within the normal range in EBV-B cells stimulated with IFN-α and IL-21, respectively (Fig. S4P). Accordingly, the induction of target genes (*CXCL10* and *SOCS3*) in patients' EBV-B cells stimulated with IFN-α or IL-21 was normal (Fig. S4Q), as was that in patients' SV40 fibroblasts stimulated with IFN-α or IL-6/IL-6Rα (Fig. S4R). Overall, immortalized cell lines from the patients displayed no major STAT3 phenotype, with the possible exception of slightly low levels of STAT3 mRNA and protein in HVS-T cells and SV40-fibroblasts.

STAT3 function is impaired in ZNF341-deficient primary fibroblasts

Some ZNF341-deficient patients displayed non-hematopoietic features seen in AD-HIES patients, such as facial dysmorphia (P6 and P7), joint hyperextensibility (P6 and P8), recurrent bone fractures (P7), jaw and tooth abnormalities (P3 and P5), and a high palate (P4, P5, P6 and P7). We therefore analyzed the impact of ZNF341 deficiency in primary fibroblast cell lines. We evaluated *STAT3* mRNA levels by RT-qPCR, and protein levels by flow cytometry and western blotting. We found that STAT3 levels were about 50% lower in the patients' fibroblasts (n=3) than in fibroblasts from healthy controls (Fig. 5A-B, Fig. S5A). We then assessed the impact of the STAT3-activating cytokine IL-6. After 30 minutes of costimulation with IL-6 and soluble IL-6Rα (hereafter referred to as IL-6/IL-6Rα), STAT3 phosphorylation was ~60% lower in ZNF341-deficient fibroblasts than in WT fibroblasts (Fig. 5C). Low levels of STAT3 phosphorylation were associated with weaker (p=0.06) *SOCS3* mRNA induction after two hours of stimulation (Fig. 5D). The activation of STAT3 by IL-6 in murine cells or the human HepG2 cell line upregulates expression of the *STAT3* gene itself (37, 38). Following IL-6/IL-6Rα treatment, we observed a weak induction of *STAT3* mRNA in patients' cells, relative to control cells (Fig. S5B). These data indicate that ZNF341 deficiency results in low baseline levels of STAT3 mRNA and protein, together with impaired STAT3 phosphorylation and transcriptional activity, in primary fibroblasts, and, by inference, perhaps in other non-hematopoietic cell types. These experiments provide a mechanism of action of ZNF341, and a mechanism of disease in the studied AR-HIES patients, by functionally connecting the ZNF341 deficit with *STAT3*, which is mutated in patients with AD-HIES. These data also explain the extrahematopoietic features observed in some patients. The somewhat rarer and milder non-hematopoietic features of ZNF341-deficient patients than of patients with DN *STAT3* DN mutations may reflect a certain level of redundancy of ZNF341 in some cell types.

STAT3 function is normal in ZNF341-deficient monocytes

Another particular feature of AR ZNF341 deficiency, differentiating this condition from AD STAT3 deficiency, is the apparently stronger inflammatory response during infection. As monocytes from healthy donors contain the ZNF341 protein (Fig. 2J), we analyzed the impact of ZNF341 deficiency in primary monocytes. We found low levels of STAT3 mRNA and protein in the monocytes of ZNF341-deficient patients, as shown by RT-qPCR and flow cytometry (Fig 5E, F). Moreover, STAT3 phosphorylation levels were ~50% lower in ZNF341-deficient monocytes following stimulation with IL-10, a STAT3-activating cytokine, than in control cells (Fig. 5G). Monocyte IL-10 signaling is impaired in STAT3-DN patients (6). We therefore measured *SOCS3* mRNA induction in monocytes from five controls, P4, and P5, after two hours of IL-10 stimulation. Levels of *SOCS3* mRNA induction were found to be normal in the patients (Fig. 5H). We then studied TNF production by fresh monocytes from healthy controls (n=9), STAT3-DN patients (n=3), and P4 in response to LPS stimulation, alone or in the presence of IL-10 (Fig. 5I). As expected, IL-10 inhibited TNF production upon LPS activation in monocytes from controls, but not in monocytes from the STAT3-DN patients. By contrast, the IL-10-mediated inhibition of TNF production in P4 monocytes upon LPS stimulation was reproducibly intact, suggesting that ZNF341 deficiency had no effect on STAT3-dependent responses to IL-10, and, by inference, to other cytokines, in these cells, as shown for IL-6 (Fig S5C). These findings

indicate that low baseline levels of STAT3 do not necessarily lead to low levels of STAT3 activity in ZNF341-deficient cells, although monocytes and fibroblasts differ in this respect. This experiment also provided an explanation for the stronger inflammation observed in ZNF341-deficient patients than in STAT3-DN patients.

STAT3 production and activation are impaired in ZNF341-deficient cytotoxic lymphocytes

ZNF341-deficient patients have low NK cell counts and low frequencies of central memory $CD8^+$ T cells. Both these cell types expressed ZNF341 in healthy controls (Fig. 2I). We analyzed the impact of ZNF341 deficiency in the remaining primary NK cells and in naïve $CD8^+$ T cells, analyzing the expression and activation of STAT3 (Fig. 5J-M, Fig. S5D-F). We tested STAT3 expression by flow cytometry in $CD56^{dim}$ NK cells and in naïve $CD8^+$ T cells, and found that STAT3 expression was decreased in the patients by about 50% in both subsets, when compared with healthy controls (Fig. 5J-L). After IL-21 stimulation, STAT3 phosphorylation was decreased by ~40 % and 60% in ZNF341-deficient $CD56^{dim}$ NK cells and naïve $CD8^+$ T cells, respectively, relative to controls (Fig. 5K, M). Normal NK cell numbers in STAT3-DN patients suggests that low STAT3 expression and function in ZNF341 deficient NK cells is unlikely to explain their NK cell lymphopenia. In contrast, the similarly low frequency of central memory $CD8^+$ T cells in ZNF341-deficient patients and patients with DN *STAT3* mutations suggests that low STAT3 expression and function is responsible for impaired central memory $CD8^+$ T cell differentiation in ZNF341-deficient patients. Collectively, these findings showed that the impact of ZNF341 deficiency, in terms of STAT3 baseline expression and inducible activation, extended beyond fibroblasts and monocytes to cytotoxic NK and $CD8^+$ T cells. However, we did not test STAT3 activity in these two cell types.

STAT3 activity is impaired in ZNF341-deficient B cells

We next analyzed the impact of ZNF341 deficiency in primary naïve and memory B-lymphocytes. Compared with controls, STAT3 expression was decreased in patients' primary naïve B cell subsets by about 50%, as determined by flow cytometry (Fig 5N, Fig. S5G). After IL-21 stimulation, STAT3 phosphorylation was decreased by ~50% in naïve B cells from ZNF341-deficient patients, when compared with controls (Fig. 5O, Fig. S5H). We assessed *STAT3* induction in naïve B cells from controls, a STAT3-DN patient, and a ZNF341-deficient patient (P8), upon stimulation with CD40L with or without IL-21 (Fig. 5P). Stimulation for four hours with CD40L alone induced a transient tripling of *STAT3* mRNA levels in controls and patients (Fig. 5P). Incubation with CD40L plus IL21 induced a ~10 fold increase in *STAT3* mRNA levels in naïve B cells from controls, after 4 hours of stimulation, demonstrating synergy between the CD40L and IL-21 pathways (Fig. 5P). In contrast, naïve B cells from ZNF341-deficient patient displayed no such induction after stimulation with CD40L and IL-21 (Fig. 5P). Normal induction was detected with STAT3-DN naïve B cells, suggesting that the residual STAT3 activity in these cells was sufficient to induce *STAT3* mRNA upregulation upon costimulation with CD40L and IL-21 (Fig. 5P). As ZNF341-deficient patients have selectively high serum IgG and IgE levels, and high levels of allergen-specific IgE (Fig. S5I), together with memory B-cell deficiency, we investigated the ability of their B cells to secrete Ig in various culture conditions requiring STAT3 activation. We sorted naïve and memory B cells from controls and patients and cultured

them for seven days in the presence of CD40L, alone or together with IL-21 (Fig. 5Q, R). The induction of IgM, IgG, and IgA secretion by naive B cells from the patients in response to stimulation with CD40L and IL-21 was severely impaired (<0.1–10% of normal levels) (Fig. 5Q). By contrast, the levels of IgM and IgA secretion by ZNF341-deficient memory B cells were 10–30% those in controls, whereas the secretion of IgG was unaffected (Fig. 5R). Naïve and memory B cells from the patients produced normal levels of IgM in response to CD40L/CpG/BCR engagement (used as a control) (Fig. S5J). These data closely resemble published findings for patients with AD HIES due to DN *STAT3* mutations (5, 18). It strongly suggests that ZNF341 deficiency in circulating naïve B cells affects their function, by preventing these cells from responding to IL-21 via STAT3. These findings may explain the B-cell phenotype observed in both ZNF341- and STAT3-mutated patients with HIES. They also suggest that impairment of the auto-induction of STAT3 (i.e. the induction of STAT3 mRNA and protein by phosphorylated STAT3 dimers) is a critical mechanism underlying the pathogenesis of ZNF341 deficiency.

STAT3 auto-induction is impaired in ZNF341-deficient naïve CD4$^+$ T cells

We then assessed the impact of ZNF341 deficiency in primary CD4$^+$ T lymphocytes. Steady-state endogenous levels of STAT3 mRNA and protein were about 50% lower in the patients' (P2, P3, and P4) naïve CD4$^+$ T cells than in those of healthy controls (Fig. 6A, B). These low levels of STAT3 were associated with lower levels of IL-6/IL-6Rα-induced STAT3 phosphorylation (~65%) (Fig. 6C). The auto-induction of *Stat3* in mice is observed in T cells, in which it enhances cell proliferation and survival upon CD3 and IL-6 co-stimulation (38). Furthermore, impaired auto-induction of *Stat3* was reported in mouse PKC-θ deficient naïve CD4$^+$ T cells upon TCR stimulation with Th17 polarizing cytokines, disrupting Th17 cell differentiation (39). We therefore assessed *STAT3* induction in naïve CD4$^+$ T cells from controls, STAT3-DN patients, and ZNF341-deficient patients (P4, P5 and P7), upon stimulation with anti-CD2/CD3/CD28 mAb-coated beads (Th0) with or without IL-6/IL-6Rα or Th17-polarizing cytokines (TGF-β, IL-1β, IL-6, IL-21 and IL-23) (Fig. 6D, Fig. S6A). Stimulation for two or four hours with IL-6/IL-6Rα, anti-CD2/CD3/CD28 mAb-coated beads, or Th17-polarizing cytokines alone induced a transient two- to six-fold increase in *STAT3* mRNA levels, peaking after two hours of stimulation in controls (Fig. 6D, Fig. S6A). Incubation with anti-CD2/CD3/CD28 mAb-coated beads plus IL-6/IL-6Rα or Th17-polarizing cytokines induced a 10- to 20-fold increase in *STAT3* mRNA levels in naïve CD4$^+$ T cells from controls, after 2 hours of stimulation, demonstrating a potent synergy between the CD2/CD3/CD28 and IL-6R pathways (Fig. 6D, Fig. S6A). By contrast to the four STAT3-activating cytokines tested — IL-6 and IL-21 (STAT3), IFN-α and IFN-γ (STAT1 and STAT3) — the IL-2, IL-4, and IL-12 cytokines, which activate STAT5, STAT6, and STAT4, respectively, induced no such synergy (Fig. S6B). Strikingly, naïve CD4$^+$ T cells from ZNF341-deficient patients displayed no such synergy after stimulation with anti-CD2/CD3/CD28 mAb-coated beads plus IL-6/IL-6Rα or Th17-polarizing cytokines (Fig. 6D, Fig. S6A). Normal synergy was detected with STAT3-DN naïve CD4$^+$ T cells, suggesting that the residual STAT3 activity in these cells was sufficient to induce *STAT3* mRNA upregulation upon costimulation (Fig. 6D, Fig. S6A). We compared the transcriptomes of naïve CD4$^+$ T cells from four controls and two patients (P4 and P7) on microarrays, after two hours of costimulation with anti-CD2/CD3/CD28 mAb-coated beads

and IL-6/IL-6Rα. Relevant cytokine receptor mRNAs (i.e. *IL2RG*, *IL6R*, *IL6ST*, *IL21R,* and *IL23R*) were present at normal levels in the patients' cells, suggesting that the impairment of STAT3 induction was not due to impaired cytokine receptor expression. Only three and 65 transcripts showed a fold-change in expression (FC; mean mRNA level of patients/mean mRNA level of controls) of less than 0.4 or more than 2.5, respectively (Table S6). Strikingly, of the three genes underexpressed in patient, *STAT3* displayed the largest decrease in expression in patients (FC = 0.34), demonstrating that the lack of ZNF341 resulted primarily in a decrease in *STAT3* mRNA induction in the patients' cells. Conversely, of the 65 genes less strongly expressed in controls than in patients following costimulation, the largest difference in mRNA levels was observed for *IFNG* (FC=11.6). This finding is consistent with the higher levels of IFN-γ expression observed in naïve $CD4^+$ T cells from STAT3-DN patients than in control cells, after stimulation with anti-CD2/CD3/CD28 mAb-coated beads and Th1-polarizing cytokines (22). We investigated *STAT3* autoregulation in naïve $CD4^+$ T cells further, by assessing the impact of four hours of stimulation with anti-CD2/CD3/CD28 mAb-coated beads, IL-6, or both, on STAT3 protein production, phosphorylation, and localization (Fig. 6E). STAT3 and p-STAT3 levels were higher in the nucleus of control naïve $CD4^+$ T cells after 4 hours of costimulation, than after stimulation with IL-6/IL-6Rα or anti-CD2/CD3/CD28 mAb-coated beads alone. This increase was affected by cycloheximide treatment, suggesting that *STAT3* mRNA auto-induction is associated with the *de novo* synthesis of STAT3 protein (Fig. 6E). Moreover, costimulation with anti-CD2/CD3/CD28 mAb-coated beads and IL-6/IL-6Rα resulted in long-lasting *SOCS3* mRNA induction in naïve control $CD4^+$ T cells (Fig. 6F). Accordingly, the induction of *SOCS3* mRNA was impaired in ZNF341-deficient patients after two and four hours of costimulation (Fig. 6G and Fig. S6C). Finally, we found that basal *ZNF341* mRNA levels were normal in STAT3-DN naïve $CD4^+$ T cells, but high in ZNF341-deficient cells (Fig. 6H), further suggesting that ZNF341 autoregulates its own expression (Fig. 2D). Consistent with this finding, we detected a strong ZNF341-binding site in the first intron of *ZNF341* by ChIP-Seq (Fig. 4B). Two hours of IL-6/IL-6Rα stimulation in ZNF341-deficient naïve $CD4^+$ T cells restored normal *ZNF341* mRNA levels, suggesting that STAT3 may also regulate *ZNF341* expression (Fig. 6H). Overall, these data show that ZNF341 is required for baseline STAT3 production, auto-induction, activation, and sustained activity in primary human T cells.

Th17 development is impaired in ZNF341-deficient patients

We investigated the mechanism underlying CMC in ZNF341-deficient patients, by analyzing the development of IL-17^+ $CD4^+$ T cells. Inborn errors of IL-17 immunity underlie all known forms of isolated or syndromic CMC (21, 40–46), including HIES due to DN *STAT3* mutations (14, 20, 47, 48). The proportions of Th subsets among the circulating memory $CD4^+$ T cells of ZNF341-deficient patients were normal for Th1 cells, high for Th2 cells, and low for Tfh, Th1*, and Th17 cells, as shown by the expression of specific surface markers (Fig. 7A), as in STAT3 DN patients (49, 50). We stimulated memory $CD4^+$ T cells with anti-CD2/CD3/CD28 mAb-coated beads (Th0) for five days, and measured cytokine production by ELISA, cytometric bead array, and intracellular staining methods (Fig. 7B and Fig. S7A-C). The production of Th1 cytokines (TNF, IFN-γ) was low to normal (Fig. 7B, Fig. S7A), and that of IL-6, IL-10 and IL-21 was normal (Fig. S7B,C), whereas that of Th2

cytokines (IL-4, IL-5, IL-13) was normal or higher than normal (Fig. 7B, Fig. S7A). In marked contrast, the production of Th17 cytokines (IL-17A, IL-17F, IL-22) by ZNF341-deficient memory CD4$^+$ T cells was much weaker than that by control cells (Fig. 7B, Fig. S7A). We then purified naïve CD4$^+$ T cells from the patients and cultured them *in vitro* under Th1- or Th17-polarizing conditions. Th1 polarization induced normal and high levels of TNF and IFN-γ, respectively, in the patients' cells (Fig. S7D), consistent with the microarray data (Table S6) and similar to the results obtained for STAT3-DN patients (22). By contrast, Th17 polarization did not lead to the production of detectable amounts of IL-17A and IL-17F (Fig. 7C). Accordingly, *RORC* expression tended to be weaker, although this difference was not statistically significant, in memory CD4$^+$ T cells and naïve CD4$^+$ T cells from patients cultured for five days under Th17 conditions *in vitro* (Fig. 7D). These data are consistent with the ChIP-seq data for T cells, in which no ZNF341 binding site was detected in the *RORC* gene. By contrast, the expression of *TBX21* and *GATA3* was normal or slightly higher than normal in memory CD4$^+$ T cells and naïve CD4$^+$ T cells from patients cultured under Th1- and Th2-polarizing conditions, respectively (Fig. 7D). Mutations of *ZNF341* may have had a global effect on T-cell responses, impairing not only responses elicited through cytokine receptors, but also those elicited through the TCR. We tested this hypothesis, by measuring the calcium flux in naïve CD4$^+$ T cells induced by TCR engagement (Fig. S7E). The kinetics and magnitude of the TCR-mediated activation of naïve CD4$^+$ T cells from two ZNF341-deficient patients were similar to those of corresponding cells from healthy donors, suggesting that TCR signaling was intact in the absence of ZNF341. Furthermore, ZNF341-deficient naïve and memory CD4$^+$ T cells underwent rounds of normal proliferation *in vitro* in response to Th0 or polarizing conditions (Fig. S7F,G). The IL-17 phenotype observed in ZNF341-deficient patients was not, therefore, due to impaired cell division and TCR-induced calcium signaling.

Patients' Th cells show an abnormal transcriptome profile

The patients' CD4$^+$ T cells were further studied globally by gene expression analysis (Fig. S7H). Consistent with the skewing towards Th2 cells, ZNF341-deficient memory CD4$^+$ T cells had higher levels of mRNAs encoding not only GATA3, IL-4, IL-5, and IL-13, but also IL-5R, IL-31 (produced by Th2 cells), and IL-18BP (inhibiting IL-18-induced IFN-γ production, thereby relieving the inhibitory effect of IFN-γ on Th2 responses). Remarkably, ZNF341-deficient memory CD4$^+$ T cells continued to produce large amounts of *GATA3*, *IL4*, *IL13* and *IL31* under Th17-polarizing conditions. Moreover, ZNF341-deficient memory CD4$^+$ T cells had lower basal levels of *IL17A*, *IL17F*, *IL22* and *CCR6* expression under Th0 conditions than control memory CD4$^+$ T cells, and the expression of *IL17A*, *IL17F,* and *CCR6* was not increased by culturing ZNF341-deficient memory CD4$^+$ T cells under Th17 conditions (Fig. S7H). Impaired expression was also observed for other genes typically associated with Th17 cells, including *RORA* (encoding ROR-α), *IL26*, *CCL20* (both expressed by human Th17 cells), *IL23A*, *IL1A*, *IL1R1*, *IL1R2*, *IL6R* and *IL23R* (which encode proteins through which IL-1β, IL-6 and IL-23 signal to induce Th17 cells). The increase in *RORC*, *CCL20*, *IL1A*, *IL1R1*, *IL1R2* and *IL23A* expression observed in normal memory CD4$^+$ T cells after culture in Th17-polarizing conditions was abolished by *ZNF341* mutations, highlighting the key role of this transcription factor in Th17 differentiation. Consistently, total RNA sequencing in isolated CD3+ T cells from P4 and a control after 24

and 48 hours of stimulation with anti-CD3 and anti-CD28 mAbs revealed that six of the ten genes for which the most significant decreases in expression were recorded in patients were key markers of IL-17 immunity (*IL17A*, *IL17F*, *IL26*, *RORC*, *CCL20*, *CCR6*; Table S7 and not shown). In summary, ZNF341-deficient $CD4^+$ T cells can differentiate *in vivo* and *in vitro* into some types of effector cells, but their ability to generate Th17 cells is selectively and severely impaired. As in patients with DN *STAT3* mutations, this defect accounts for the CMC observed in the patients, as fibroblasts and keratinocytes from P2–P4 responded normally to IL-17A (Fig. S7I-K) (21, 44–46). The lack of ZNF341 prevents Th cells from producing sufficient amounts of functional STAT3, and thereby of ROR-γ/ROR-γT, during Th17 development (14, 42).

Allergy and hyper-IgE are associated with enhanced Th2 responses

Unlike the CMC observed in patients and our findings for IL-17, the pathogenesis of severe allergy and hyper-IgE in these patients is more difficult to decipher, as monogenic causes of isolated allergy and hyper-IgE affecting specific cytokine signaling pathways are only just beginning to emerge (51, 52). However, the microarray analysis of $CD4^+$ T cells was instructive, revealing aberrant expression of potential mediators of inflammation in ZNF341-deficient patients (Fig. S7H). We detected high levels of expression of the inflammatory chemokine genes *CCL1*, *CCL3*, *CCL5*, and the inflammatory chemokine receptor gene *CXCR3*, which is co-expressed by Th1 cells. This finding is consistent with the detection of high levels of expression for *IFNG* and *EOMES*, encoding a transcription factor required for the generation of pathogenic pro-inflammatory IFN-γ-producing $CD4^+$ T cells. The persistently higher levels of expression of many of these inflammatory or Th2-type genes in ZNF341-deficient than in control memory $CD4^+$ T cells under conditions of Th17 polarization also highlight the role of ZNF341 in repressing the expression of gene signatures characteristic of alternative fates of effector $CD4^+$ T cells. The patients thus displayed an enhanced Th2 bias in multiple assays (Fig. 7B and Fig. S7A), with a higher frequency of Th2 cells and higher levels of *GATA3* mRNA in memory $CD4^+$ T cells (Fig. 7A, D). Finally, we tested the hypothesis that the patients' $CD8^+$ T cells also contributed to their allergic phenotype (53, 54). Genome-wide transcriptome analysis showed that up to 12 mRNAs were upregulated in the patients' $CD8^+$ HVS-T cells, to levels at least 2.5 times those in $CD8^+$ HVS-T cells from healthy controls (Fig. S7L). Two of these genes encoded cytokines known to play a key role in the allergy process: IL-5, which drives the development of eosinophils (55), and IL-9, which drives the development of basophils (56). These data suggest that the allergic features of ZNF341-deficient patients were due to the enhanced production of some, but not all Th2-like cytokines, including IL-5 and IL-9, in particular, by both $CD4^+$ and $CD8^+$ T cells. These T-cell abnormalities are similar to those seen in HIES patients with DN mutations of *STAT3* (22, 50).

Discussion

We report ZNF341 deficiency in eight patients from six unrelated kindreds displaying an AR form of HIES, with stronger inflammatory responses and fewer non-hematopoietic manifestations than reported for AD HIES caused by DN *STAT3* mutations. This experiment of nature indicates that human ZNF341 is required for protective mucocutaneous immunity

to *Candida albicans*. The impaired development of IL-17$^+$ CD4$^+$ T cells accounts for the development of CMC in these patients (7, 14, 20, 40–43, 47, 48). The cellular mechanisms by which ZNF341 regulates allergy are less clear, although several Th2 cytokines (e.g. IL-5, IL-9) are produced in excess by the patients' T cells. The molecular mechanism by which ZNF341 operates in T cells involves STAT3. No haploinsufficiency has been observed at the human *STAT3* locus; the HIES-causing *STAT3* mutations studied to date are all DN (6, 57, 58). The mechanism by which ZNF341 deficiency is pathogenic in T cells is based on a 50% decrease in constitutive levels of STAT3, and a >60% decrease in levels of STAT3 phosphorylation upon stimulation with STAT3-activating cytokines. ZNF341 deficiency prevents the induction of *STAT3* transcription by cytokines that activate STAT3 itself (auto-induction). Together, low baseline STAT3 mRNA and protein levels, and the impaired auto-induction of STAT3 itself, result in lower levels of STAT3 activation (phosphorylation) and transcriptional activity, as low as those in patients with DN *STAT3* mutations. Consequently, STAT3-dependent genes, such as *RORC*, *IL17A,* and *IL17F,* are poorly induced. Consistent with these findings, the overexpression of a hyperactive form of *STAT3* in naïve mouse CD4$^+$ T cells and *STAT3* gain-of-function mutations in humans were shown to increase Th17 cell differentiation (59, 60). The same mechanism probably operates in B cells, accounting for the B-cell phenotypes of ZNF341-deficient patients being identical to those of HIES patients with DN *STAT3* mutations (5, 18). Given that patients with the various forms of inherited STAT1 deficiency suffer from mycobacterial and/or viral diseases (61), and that individuals heterozygous for LOF *STAT1* alleles that are not DN are asymptomatic, the lower levels of STAT1 observed in ZNF341-deficient patients are unlikely to account for or even contribute to their immunological or clinical phenotypes.

Patients with ZNF341 deficiency appear to develop fewer and milder non-hematopoietic developmental phenotypes than patients with *STAT3* DN mutations. A possible explanation for this is that IL-11R, LIFR, IL-6ST, and similar receptors in cells responsible for the tooth, skeletal, joint, and vascular phenotypes of AD HIES patients may not necessarily require as much STAT3 to function properly as the cytokine receptors tested in primary fibroblasts (10–12). However, these patients do develop such somatic features, consistent with the STAT3 phenotype detected in the fibroblasts of ZNF341-deficient patients. One of the more distinctive features of ZNF341 deficiency is the somewhat stronger inflammatory response in the course of infection. We detected ZNF341 in all leukocytes tested, including basophils, monocytes, and dendritic cells. However, the expression of this protein in monocytes seems to be functionally redundant for STAT3 activation, by contrast to the situation in STAT3-DN patients, possibly explaining the normal biological and clinical inflammation seen in ZNF341-deficient patients. Conversely, the NK lymphopenia seen in ZNF341-deficient but not STAT3-DN patients suggests that ZNF341 may be essential for at least one STAT3-independent function. However, an alternative interpretation is that STAT3 activation is more profoundly impaired in NK progenitors lacking ZNF341 than in those carrying a DN *STAT3* mutation. Further studies will be required to compare the expression patterns of ZNF341 and STAT3 proteins across human tissues and cell types. Studies of *Zfp341*, the mouse ortholog of human *ZNF341*, may also facilitate analysis of the STAT3-dependent and STAT3–independent roles of this transcription factor in different cell types.

The identification of ZNF341 highlights the power of human genetics for discovering new biochemical and immunological pathways of biological and medical relevance (62–64) and defining the level of redundancy of human genes for host defense in natural conditions (65). Much is already known about the structure and function of STAT proteins, but this study reveals the importance of the transcriptional regulation of *STAT* genes (66–69). Previous studies had hinted at the importance of STAT transcriptional regulation (37–39). Unlike STAT3, which resides in the cytosol and only accumulates in the nucleus upon activation, ZNF341 is constitutively expressed in the nucleus, where it is required for optimal baseline and inducible *STAT3* transcription, and particularly for auto-induction, the lack of which prevents the production of sufficient amounts of STAT3 protein and the sustained activity of this protein during cell stimulation. Further studies are required to identify potential partners of ZNF341 during STAT3 auto-induction. In T and B cells, we have further shown that ZNF341 protein deficiency is associated with higher levels of *ZNF341* mRNA. Both ZNF341 and STAT3 are potent inducers of *STAT3* transcription, and they may act in concert to decrease *ZNF341* transcription. This would prevent excessive STAT3-dependent responses that would be deleterious to the host, as observed in patients with heterozygous gain-of-function mutations of *STAT3* (70–72).

Materials and methods

Study design

We studied eight patients from five kindreds suffering from HIES. Using whole exome sequencing, we found that all living patients carry homozygous truncating mutation in the *ZNF341* gene. No predicted homozygous LOF mutation of *ZNF341* has ever been described in public databases. ZNF341 function is unknown in mouse and human. The main objective of this study was to characterize in depth ZNF341 expression and function in human, and the molecular, cellular, and immunological impacts of its disruption in human.

Case reports

Detailed case reports of all eight patients can be found in the Supplementary Material.

Experimental methods

Information about reagents used and experimental procedures can be found in the Supplemental Material.

Statistics

Two-tailed Mann-Whitney tests or unpaired t tests were used for single comparisons of independent groups. Paired t test were used for single comparisons of paired groups. In the relevant figures, n.s. indicates not significant; ***$p < 0.001$; **$p < 0.01$; and *$p < 0.05$. Analyses were performed with GraphPad software.

Supplementary Material

Refer to Web version on PubMed Central for supplementary material.

Authors

Vivien Béziat[1,2,*], Juan Li[#3], Jian-Xin Lin[#4], Cindy S. Ma[#5,6], Peng Li[#4], Aziz Bousfiha[#7], Isabelle Pellier[#8], Samaneh Zoghi[#9,10,11], Safa Baris[#12], Sevgi Keles[#13], Paul Gray[#14,15], Ning Du[#4], Yi Wang[#1,2], Yoann Zerbib[#1,2], Romain Lévy[#1,2], Thibaut Leclercq[#1,2], Frédégonde About[1,2], Ai Ing Lim[16,17], Geetha Rao[5], Kathryn Payne[5], Simon J Pelham[5,6], Danielle T Avery[5], Elissa K Deenick[5,6], Bethany Pillay[5,6], Janet Chou[18,19], Romain Guery[1,2,20], Aziz Belkadi[1,2], Antoine Guérin[1,2], Mélanie Migaud[1,2], Vimel Rattina[1,2], Fatima Ailal[7], Ibtihal Benhsaien[7], Mathieu Bouaziz[1,2], Habib Tanwir[21], Damien Chaussabel[21], Nico Marr[21], Jamel El Benna[22], Bodo Grimbacher[23], Orli Wargon[24], Jacinta C. Bustamante[1,2,3,25], Bertrand Boisson[1,2,3], Ingrid Müller-Fleckenstein[26], Bernhard Fleckenstein[26], Marie-Olivia Chandesris[27,28], Matthias Titeux[2,29], Sylvie Fraitag[30], Marie-Alexandra Alyanakian[31], Marianne Leruez-Ville[32], Capucine Picard[1,2,25], Isabelle Meyts[33], James P. Di Santo[16,17], Alain Hovnanian[#2,29,34], Ayper Somer[#35], Ahmet Ozen[#12], Nima Rezaei[#9,10], Talal Chatila[#18,19], Laurent Abel[#1,2,3], Warren J. Leonard[#4], Stuart G. Tangye[#5,6], Anne Puel[#1,2,3,*], and Jean-Laurent Casanova[#1,2,3,36,37,*]

Affiliations

[1.] Laboratory of Human Genetics of Infectious Diseases, Necker Branch, INSERM U1163, 75015 Paris, France, EU.

[2.] Paris Descartes University, Imagine Institute, 75015 Paris, France, EU.

[3.] St. Giles Laboratory of Human Genetics of Infectious Diseases, Rockefeller Branch, The Rockefeller University, New York, NY 10065, USA.

[4.] Laboratory of Molecular Immunology and the Immunology Center, NHLBI, NIH, Bethesda, MD 20892-1674, USA.

[5.] Immunology Division, Garvan Institute of Medical Research, Darlinghurst, Sydney, NSW 2010, Australia.

[6.] St. Vincent's Clinical School, UNSW Sydney, Sydney, NSW 2052, Australia.

[7.] Clinical Immunology Unit, Casablanca Children's Hospital, Ibn Rochd Medical School, King Hassan II University, Casablanca, Morocco.

[8.] Pediatric Hemato-Oncology Unit, University Hospital of Angers, 49933 Angers, France, EU.

[9.] Research Center for Immunodeficiencies, Children's Medical Center, Tehran University of Medical Sciences, 1417613151 Tehran, Iran.

[10.] Network of Immunity in Infection, Malignancy and Autoimmunity (NIIMA), Universal Scientific Education and Research Network (USERN), 1419733151 Tehran, Iran.

[11.] Department of Immunology, School of Medicine, Tehran University of Medical Sciences, Tehran, Iran.

[12.] Marmara University, Division of Pediatric Allergy/Immunology, 34722 Istanbul, Turkey.

[13.] Necmettin Erbakan University, Meram Medical Faculty, Division of Pediatric Allergy and Immunology, 42060 Konya, Turkey.

[14.] Department of Immunology and Infectious Diseases, Sydney Children's Hospital, Randwick, New South Wales 2031, Australia

[15.] School of Women's and Children's Health, University of New South Wales School of Women's and Children's Health, Sydney, New South Wales 2031, Australia

[16.] Innate Immunity Unit, Institut Pasteur, 75015 Paris, France, EU.

[17.] INSERM U1223, 75015 Paris, France, EU.

[18.] Division of Immunology, Boston Children's Hospital, Boston, MA 02115, USA.

[19.] Department of Pediatrics, Harvard Medical School, Boston, MA 02115, USA.

[20.] Unit of Tropical and Infectious Diseases, Necker Hospital for Sick Children, AP-HP, 75015 Paris, France, EU.

[21.] Sidra Medical and Research Center, Doha, Qatar.

[22.] INSERM-U1149, CNRS-ERL8252, Center for Research on Inflammation, Labex Inflamex, Paris Diderot University, Faculté de Médecine, Xavier Bichat Medical School, 75018 Paris, France.

[23.] Center for Chronic Immunodeficiency (CCI), Medical Center, Faculty of Medicine, University of Freiburg, 79106 Freiburg, Germany.

[24.] Dept of Paediatric Dermatology, Sydney Children's Hospital, High St Randwick NSW 2031, Australia

[25.] Study Center for Immunodeficiency, Necker Hospital for Sick Children, AP-HP, 75015 Paris, France, EU.

[26.] Institute of Clinical and Molecular Virology, University of Erlangen-Nürnberg, D-91054 Erlangen, Germany, EU.

[27.] Department of Hematology, Necker Hospital for Sick Children, AP-HP, 75015 Paris, France, EU.

[28.] Referral Center for Immunodeficiency, Necker Hospital for Sick Children, AP-HP, 75015 Paris, France, EU.

[29.] Laboratory of Genetic Skin Diseases: from Disease Mechanism to Therapies, INSERM U1163, 75015 Paris, France, EU.

[30.] Department of Pathology, Necker Hospital for Sick Children, AP-HP, 75015 Paris, France, EU.

[31.] Immunology Laboratory, Necker Hospital for Sick Children, AP-HP, 75015 Paris, France, EU.

[32.] Virology Laboratory, Necker Hospital for Sick Children, AP-HP, 75015 Paris Descartes University, EA 73-28, 75015 Paris, France, EU.

[33.] Department of Immunology and Microbiology, Childhood Immunology, Department of Pediatrics, University Hospitals Leuven and KU Leuven, 3000 Leuven, Belgium, EU.

[34.] Department of Genetics, Necker Hospital for Sick Children, AP-HP, 75015 Paris, France, EU.

[35.] Istanbul University, Istanbul Medical Faculty, Division of Infectious Diseases and Immunology, 34452 Istanbul, Turkey.

[36.] Pediatric Hematology-Immunology Unit, Necker Hospital for Sick Children, AP-HP, 75015 Paris, France, EU.

[37.] Howard Hughes Medical Institute, New York 10065, USA.

Acknowledgments

We would like to thank the patients and their families for participating in this study. We thank James E. Darnell and Claudia Mertens for advice and for providing reagents. We thank the members of the laboratory, especially Fabienne Jabot-Hanin and Vincent Pedergnana, for their valuable input on linkage analysis; Lahouari Amar, Yelena Nemirovskaya, Dominick Papandrea, Eric Anderson, Mark Woollett, Céline Desvallées, Cécile Patissier and Michaëla Corrias for administrative assistance; Emmanuelle Jouanguy, and Yuval Itan for helpful discussions; Sébastien Jacques and the Cochin genomics platform for microarray experiments; and Nicolas Goudin and Raphaëlle Desveaux of the Necker Institute Imaging Facility.

Funding

This work was supported by grants from Institut National de la Santé et de la Recherche Médicale (INSERM), Paris Descartes University, the Integrative Biology of Emerging Infectious Diseases Laboratoire d'Excellence (ANR-10-LABX-62-IBEID), the Jeffrey Modell Foundation Translational Research Program, the French National Research Agency (ANR) (grants no. GENCMCD-ANR-11-BSV3–005–01, no. HGDIFD-ANR-14-CE15–0006-01, no. NKIR-ANR-13-PDOC-0025–01 and no. EURO-CMC-ANR-14-RARE-0005–02) and grants awarded under the "Investissement d'avenir" program (grant no.ANR-10-IAHU-01)), the National Institute of Allergy and Infectious Diseases of the National Institutes of Health (grant no. U01AI109697 and no. R01AI127564), the Rockefeller University, the Howard Hughes Medical Institute, the St. Giles Foundation, the Institut Pasteur, and FP7, under grant agreements 305578 (PathCO) and 317057 (HOMIN). We thank the Centre de Recherche Translationnelle (Institut Pasteur) for technical assistance. V.B. is supported by the ANR (grant no. NKIR-ANR-13-PDOC-0025–01). R.L. is supported by the INSERM PhD program (poste d'accueil INSERM), a Fulbright grant (Franco-American commission) and a Philippe Foundation scholarship. Y.Z. received the "médaille d'or du Centre Hospitalier Universitaire d'Amiens". Y.W. is supported by the French National Agency for Research on AIDS and Viral Hepatitis (ANRS) (grant no. 13318). F.A. holds a fellowship from Fondation pour la Recherche Médicale (FRM, grant no. FDM20140630671). A.G. is supported by an IFNGPHOX grant (no. ANR13-ISV3–0001-01) from the French National Research Agency (ANR). IM is supported by a KOOR grant from UZ Leuven, a KOF grant from KU Leuven and an International Mobility Grant from FWO Vlaanderen. S.G.T., C.S.M. and E.K.D. are supported by grants and fellowships from the National Health and Medical Research Council of Australia, and the Jeffrey Modell Foundation. A.I.L. is a scholar of the Pasteur-Paris University (PPU) International PhD program and is supported by a PhD International Training Network grant from the European Union's Seventh Framework Program under grant agreement no. 317057 (HOMIN). J.P.D. is a founder of and shareholder in AXENIS (Paris, France). T.A.C. was supported by a grant from the National Institute of Allergy and Infectious Diseases of the National Institutes of Health (5R01AI065617). S.K. was supported by a grant from the Scientific and Technological Research Council of Turkey (1059B191300622). J.-X.L., P.L., N.D., and W.J.L. were supported by the Division of Intramural Research, National Heart, Lung, and Blood Institute, NIH.

References and Notes

1. Davis S, Schaller J, Wedgwood R, Harvard MD, JOB'S SYNDROME, The Lancet 287, 1013–1015 (1966).

2. Buckley RH, Wray BB, Belmaker EZ, Extreme Hyperimmunoglobulinemia E and Undue Susceptibility to Infection, Pediatrics 49, 59–70 (1972). [PubMed: 5059313]

3. Grimbacher B, Holland SM, Gallin JI, Greenberg F, Hill SC, Malech HL, Miller JA, O'Connell AC, Puck JM, Hyper-IgE Syndrome with Recurrent Infections — An Autosomal Dominant Multisystem Disorder, N. Engl. J. Med 340, 692–702 (1999). [PubMed: 10053178]

4. Chandesris M-O, Azarine A, Ong K-T, Taleb S, Boutouyrie P, Mousseaux E, Romain M, Bozec E, Laurent S, Boddaert N, Thumerelle C, Tillie-Leblond I, Hoarau C, Lebranchu Y, Aladjidi N, Tron F, Barlogis V, Body G, Munzer M, Jaussaud R, Suarez F, Clément O, Hermine O, Tedgui A, Lortholary O, Picard C, Mallat Z, Fischer A, Frequent and Widespread Vascular Abnormalities in Human Signal Transducer and Activator of Transcription 3 Deficiency, Circ. Cardiovasc. Genet 5, 25–34 (2012). [PubMed: 22084479]

5. Avery DT, Deenick EK, Ma CS, Suryani S, Simpson N, Chew GY, Chan TD, Palendira U, Bustamante J, Boisson-Dupuis S, Choo S, Bleasel KE, Peake J, King C, French MA, Engelhard D, Al-Hajjar S, Al-Muhsen S, Magdorf K, Roesler J, Arkwright PD, Hissaria P, Riminton DS, Wong M, Brink R, Fulcher DA, Casanova JL, Cook MC, Tangye SG, B cell-intrinsic signaling through IL-21 receptor and STAT3 is required for establishing long-lived antibody responses in humans, J. Exp. Med 207, 155–71 (2010). [PubMed: 20048285]

6. Minegishi Y, Saito M, Tsuchiya S, Tsuge I, Takada H, Hara T, Kawamura N, Ariga T, Pasic S, Stojkovic O, Metin A, Karasuyama H, Dominant-negative mutations in the DNA-binding domain of STAT3 cause hyper-IgE syndrome, Nature 448, 1058–1062 (2007). [PubMed: 17676033]

7. Chandesris MO, Melki I, Natividad A, Puel A, Fieschi C, Yun L, Thumerelle C, Oksenhendler E, Boutboul D, Thomas C, Hoarau C, Lebranchu Y, Stephan JL, Cazorla C, Aladjidi N, Micheau M, Tron F, Baruchel A, Barlogis V, Palenzuela G, Mathey C, Dominique S, Body G, Munzer M, Fouyssac F, Jaussaud R, Bader-Meunier B, Mahlaoui N, Blanche S, Debre M, Le Bourgeois M, Gandemer V, Lambert N, Grandin V, Ndaga S, Jacques C, Harre C, Forveille M, Alyanakian MA, Durandy A, Bodemer C, Suarez F, Hermine O, Lortholary O, Casanova JL, Fischer A, Picard C, Autosomal dominant STAT3 deficiency and hyper-IgE syndrome: molecular, cellular, and clinical features from a French national survey, Medicine (Baltimore) 91, e1–19 (2012). [PubMed: 22751495]

8. Holland SM, DeLeo FR, Elloumi HZ, Hsu AP, Uzel G, Brodsky N, Freeman AF, Demidowich A, Davis J, Turner ML, Anderson VL, Darnell DN, Welch PA, Kuhns DB, Frucht DM, Malech HL, Gallin JI, Kobayashi SD, Whitney AR, Voyich JM, Musser JM, Woellner C, Schäffer AA, Puck JM, Grimbacher B, STAT3 Mutations in the Hyper-IgE Syndrome, N. Engl. J. Med 357, 1608–1619 (2007). [PubMed: 17881745]

9. Renner ED, Rylaarsdam S, Aňover-Sombke S, Rack AL, Reichenbach J, Carey JC, Zhu Q, Jansson AF, Barboza J, Schimke LF, Leppert MF, Getz MM, Seger RA, Hill HR, Belohradsky BH, Torgerson TR, Ochs HD, Novel STAT3 mutations, reduced TH17 cell numbers, and variably defective STAT3 phosphorylation in Hyper-IgE syndrome, J. Allergy Clin. Immunol 122, 181–187 (2008). [PubMed: 18602572]

10. Dagoneau N, Scheffer D, Huber C, Al-Gazali LI, Rocco MD, Godard A, Martinovic J, Raas-Rothschild A, Sigaudy S, Unger S, Nicole S, Fontaine B, Taupin J-L, Moreau J-F, Superti-Furga A, Merrer ML, Bonaventure J, Munnich A, Legeai-Mallet L, Cormier-Daire V, Null Leukemia Inhibitory Factor Receptor (LIFR) Mutations in Stüve-Wiedemann/Schwartz-Jampel Type 2 Syndrome, Am. J. Hum. Genet 74, 298–305 (2004). [PubMed: 14740318]

11. Nieminen P, Morgan NV, Fenwick AL, Parmanen S, Veistinen L, Mikkola ML, van der Spek PJ, Giraud A, Judd L, Arte S, Brueton LA, Wall SA, Mathijssen IMJ, Maher ER, Wilkie AOM, Kreiborg S, Thesleff I, Inactivation of IL11 Signaling Causes Craniosynostosis, Delayed Tooth Eruption, and Supernumerary Teeth, Am. J. Hum. Genet 89, 67–81 (2011). [PubMed: 21741611]

12. Schwerd T, Twigg SRF, Aschenbrenner D, Manrique S, Miller KA, Taylor IB, Capitani M, McGowan SJ, Sweeney E, Weber A, Chen L, Bowness P, Riordan A, Cant A, Freeman AF, Milner JD, Holland SM, Frede N, Müller M, Schmidt-Arras D, Grimbacher B, Wall SA, Jones EY, Wilkie AOM, Uhlig HH, A biallelic mutation in IL6ST encoding the GP130 co-receptor causes immunodeficiency and craniosynostosis, J. Exp. Med 214, 2547–2562 (2017). [PubMed: 28747427]

13. Ives ML, Ma CS, Palendira U, Chan A, Bustamante J, Boisson-Dupuis S, Arkwright PD, Engelhard D, Averbuch D, Magdorf K, Roesler J, Peake J, Wong M, Adelstein S, Choo S, Smart JM, French MA, Fulcher DA, Cook MC, Picard C, Durandy A, Tsumura M, Kobayashi M, Uzel G, Casanova JL, Tangye SG, Deenick EK, Signal transducer and activator of transcription 3 (STAT3) mutations underlying autosomal dominant hyper-IgE syndrome impair human CD8 T-cell memory formation and function, J. Allergy Clin. Immunol (2013), doi:10.1016/j.jaci.2013.05.029.

14. Ma CS, Chew GYJ, Simpson N, Priyadarshi A, Wong M, Grimbacher B, Fulcher DA, Tangye SG, Cook MC, Deficiency of Th17 cells in hyper IgE syndrome due to mutations in STAT3, J. Exp. Med 205, 1551–1557 (2008). [PubMed: 18591410]

15. Ma CS, Avery DT, Chan A, Batten M, Bustamante J, Boisson-Dupuis S, Arkwright PD, Kreins AY, Averbuch D, Engelhard D, Magdorf K, Kilic SS, Minegishi Y, Nonoyama S, French MA, Choo S, Smart JM, Peake J, Wong M, Gray P, Cook MC, Fulcher DA, Casanova JL, Deenick EK, Tangye SG, Functional STAT3 deficiency compromises the generation of human T follicular helper cells, Blood 119, 3997–4008 (2012). [PubMed: 22403255]

16. Siegel AM, Heimall J, Freeman AF, Hsu AP, Brittain E, Brenchley JM, Douek DC, Fahle GH, Cohen JI, Holland SM, Milner JD, A Critical Role for STAT3 Transcription Factor Signaling in the Development and Maintenance of Human T Cell Memory, Immunity 35, 806–818 (2011). [PubMed: 22118528]

17. Wilson RP, Ives ML, Rao G, Lau A, Payne K, Kobayashi M, Arkwright PD, Peake J, Wong M, Adelstein S, Smart JM, French MA, Fulcher DA, Picard C, Bustamante J, Boisson-Dupuis S, Gray P, Stepensky P, Warnatz K, Freeman AF, Rossjohn J, McCluskey J, Holland SM, Casanova J-L, Uzel G, Ma CS, Tangye SG, Deenick EK, STAT3 is a critical cell-intrinsic regulator of human unconventional T cell numbers and function, J. Exp. Med 212, 855–864 (2015). [PubMed: 25941256]

18. Deenick EK, Avery DT, Chan A, Berglund LJ, Ives ML, Moens L, Stoddard JL, Bustamante J, Boisson-Dupuis S, Tsumura M, Kobayashi M, Arkwright PD, Averbuch D, Engelhard D, Roesler J, Peake J, Wong M, Adelstein S, Choo S, Smart JM, French MA, Fulcher DA, Cook MC, Picard C, Durandy A, Klein C, Holland SM, Uzel G, Casanova J-L, Ma CS, Tangye SG, Naive and memory human B cells have distinct requirements for STAT3 activation to differentiate into antibody-secreting plasma cells, J. Exp. Med 210, 2739–2753 (2013). [PubMed: 24218138]

19. Kotlarz D, Ziętara N, Uzel G, Weidemann T, Braun CJ, Diestelhorst J, Krawitz PM, Robinson PN, Hecht J, Puchałka J, Gertz EM, Schäffer AA, Lawrence MG, Kardava L, Pfeifer D, Baumann U, Pfister E-D, Hanson EP, Schambach A, Jacobs R, Kreipe H, Moir S, Milner JD, Schwille P, Mundlos S, Klein C, Loss-of-function mutations in the IL-21 receptor gene cause a primary immunodeficiency syndrome, J. Exp. Med 210, 433–443 (2013). [PubMed: 23440042]

20. Minegishi Y, Saito M, Nagasawa M, Takada H, Hara T, Tsuchiya S, Agematsu K, Yamada M, Kawamura N, Ariga T, Tsuge I, Karasuyama H, Molecular explanation for the contradiction between systemic Th17 defect and localized bacterial infection in hyper-IgE syndrome, J. Exp. Med 206, 1291–1301 (2009). [PubMed: 19487419]

21. Puel A, Cypowyj S, Bustamante J, Wright JF, Liu L, Lim HK, Migaud M, Israel L, Chrabieh M, Audry M, Gumbleton M, Toulon A, Bodemer C, El-Baghdadi J, Whitters M, Paradis T, Brooks J, Collins M, Wolfman NM, Al-Muhsen S, Galicchio M, Abel L, Picard C, Casanova J-L, Chronic Mucocutaneous Candidiasis in Humans with Inborn Errors of Interleukin-17 Immunity, Science 332, 65–68 (2011). [PubMed: 21350122]

22. Ma CS, Wong N, Rao G, Nguyen A, Avery DT, Payne K, Torpy J, O'Young P, Deenick E, Bustamante J, Puel A, Okada S, Kobayashi M, Martinez-Barricarte R, Elliott M, Kilic SS, Baghdadi JE, Minegishi Y, Bousfiha A, Robertson N, Hambleton S, Arkwright PD, French M, Blincoe AK, Hsu P, Campbell DE, Stormon MO, Wong M, Adelstein S, Fulcher DA, Cook MC, Stepensky P, Boztug K, Beier R, Ikincioğullari A, Ziegler JB, Gray P, Picard C, Boisson-Dupuis S, Phan TG, Grimbacher B, Warnatz K, Holland SM, Uzel G, Casanova J-L, Tangye SG, Unique and shared signaling pathways cooperate to regulate the differentiation of human CD4+ T cells into distinct effector subsets, J. Exp. Med 213, 1589–1608 (2016). [PubMed: 27401342]

23. Giacomelli M, Tamassia N, Moratto D, Bertolini P, Ricci G, Bertulli C, Plebani A, Cassatella M, Bazzoni F, Badolato R, SH2-domain mutations in STAT3 in hyper-IgE syndrome patients result in impairment of IL-10 function, Eur. J. Immunol 41, 3075–3084 (2011). [PubMed: 21792878]

24. Glocker E-O, Kotlarz D, Klein C, Shah N, Grimbacher B, IL-10 and IL-10 receptor defects in humans, Ann. N. Y. Acad. Sci 1246, 102–107 (2011). [PubMed: 22236434]
25. Engelhardt KR, McGhee S, Winkler S, Sassi A, Woellner C, Lopez-Herrera G, Chen A, Kim HS, Lloret MG, Schulze I, Ehl S, Thiel J, Pfeifer D, Veelken H, Niehues T, Siepermann K, Weinspach S, Reisli I, Keles S, Genel F, Kutuculer N, Camcıoğlu Y, Somer A, Karakoc-Aydiner E, Barlan I, Gennery A, Metin A, Degerliyurt A, Pietrogrande MC, Yeganeh M, Baz Z, Al-Tamemi S, Klein C, Puck JM, Holland SM, McCabe ERB, Grimbacher B, Chatila TA, Large deletions and point mutations involving the dedicator of cytokinesis 8 (DOCK8) in the autosomal-recessive form of hyper-IgE syndrome, J. Allergy Clin. Immunol 124, 1289–1302.e4 (2009). [PubMed: 20004785]
26. Zhang Q, Davis JC, Lamborn IT, Freeman AF, Jing H, Favreau AJ, Matthews HF, Davis J, Turner ML, Uzel G, Holland SM, Su HC, Combined Immunodeficiency Associated with DOCK8 Mutations, N. Engl. J. Med 361, 2046–2055 (2009). [PubMed: 19776401]
27. Zhang Q, Dove CG, Hor JL, Murdock HM, Strauss-Albee DM, Garcia JA, Mandl JN, Grodick RA, Jing H, Chandler-Brown DB, Lenardo TE, Crawford G, Matthews HF, Freeman AF, Cornall RJ, Germain RN, Mueller SN, Su HC, DOCK8 regulates lymphocyte shape integrity for skin antiviral immunity, J. Exp. Med 211, 2549–2566 (2014). [PubMed: 25422492]
28. Zhang Q, Jing H, Su HC, Recent Advances in DOCK8 Immunodeficiency Syndrome, J. Clin. Immunol 36, 441–449 (2016). [PubMed: 27207373]
29. Zhang Q, Boisson B, Béziat V, Puel A, Casanova J-L, Human hyper-IgE syndrome: singular or plural?, Mamm. Genome (2018).
30. Sassi A, Lazaroski S, Wu G, Haslam SM, Fliegauf M, Mellouli F, Patiroglu T, Unal E, Ozdemir MA, Jouhadi Z, Khadir K, Ben-Khemis L, Ben-Ali M, Ben-Mustapha I, Borchani L, Pfeifer D, Jakob T, Khemiri M, Asplund AC, Gustafsson MO, Lundin KE, Falk-Sörqvist E, Moens LN, Gungor HE, Engelhardt KR, Dziadzio M, Stauss H, Fleckenstein B, Meier R, Prayitno K, Maul-Pavicic A, Schaffer S, Rakhmanov M, Henneke P, Kraus H, Eibel H, Kölsch U, Nadifi S, Nilsson M, Bejaoui M, Schäffer AA, Smith CIE, Dell A, Barbouche M-R, Grimbacher B, Hypomorphic homozygous mutations in phosphoglucomutase 3 (PGM3) impair immunity and increase serum IgE levels, J. Allergy Clin. Immunol 133, 1410–1419.e13 (2014). [PubMed: 24698316]
31. Zhang Y, Yu X, Ichikawa M, Lyons JJ, Datta S, Lamborn IT, Jing H, Kim ES, Biancalana M, Wolfe LA, DiMaggio T, Matthews HF, Kranick SM, Stone KD, Holland SM, Reich DS, Hughes JD, Mehmet H, McElwee J, Freeman AF, Freeze HH, Su HC, Milner JD, Autosomal recessive phosphoglucomutase 3 (PGM3) mutations link glycosylation defects to atopy, immune deficiency, autoimmunity, and neurocognitive impairment, J. Allergy Clin. Immunol 133, 1400–1409.e5 (2014). [PubMed: 24589341]
32. Belkadi A, Pedergnana V, Cobat A, Itan Y, Vincent QB, Abhyankar A, Shang L, Baghdadi JE, Bousfiha A, theConsortium E, Alcais A, Boisson B, Casanova J-L, Abel L, Al-Herz W, Arikan C, Arkwright P, Aydogmus C, Bernard O, Blancas-Galicia L, Boisson-Dupuis S, Bonnet D, Stambouli OB, Boussofara L, Boutros J, Bustamante J, Ciancanelli M, Cole T, Condino-Neto A, Desai M, Fieschi C, Franco JL, Ichai P, Jouanguy E, Keser-Emiroglu M, Kilic SS, Mahdaviani SA, Mahlhoui N, Mansouri D, Parvaneh N, Picard C, Puel A, Raoult D, Rezaei N, Sanal O, Ramon SS, Vandenesch F, Vogt G, Zhang S-Y, Whole-exome sequencing to analyze population structure, parental inbreeding, and familial linkage, Proc. Natl. Acad. Sci 113, 6713–6718 (2016). [PubMed: 27247391]
33. Kircher M, Witten DM, Jain P, O'Roak BJ, Cooper GM, Shendure J, A general framework for estimating the relative pathogenicity of human genetic variants, Nat. Genet 46, 310–315 (2014). [PubMed: 24487276]
34. Itan Y, Shang L, Boisson B, Ciancanelli MJ, Markle JG, Martinez-Barricarte R, Scott E, Shah I, Stenson PD, Gleeson J, Cooper DN, Quintana-Murci L, Zhang S-Y, Abel L, Casanova J-L, The mutation significance cutoff: gene-level thresholds for variant predictions, Nat. Methods 13, 109–110 (2016). [PubMed: 26820543]
35. Cokol M, Nair R, Rost B, Finding nuclear localization signals, EMBO Rep 1, 411–415 (2000). [PubMed: 11258480]
36. Goldberg T, Hamp T, Rost B, LocTree2 predicts localization for all domains of life, Bioinformatics 28, i458–i465 (2012). [PubMed: 22962467]

37. Ichiba M, Nakajima K, Yamanaka Y, Kiuchi N, Hirano T, Autoregulation of the Stat3 Gene through Cooperation with a cAMP-responsive Element-binding Protein, J. Biol. Chem 273, 6132–6138 (1998). [PubMed: 9497331]

38. Narimatsu M, Maeda H, Itoh S, Atsumi T, Ohtani T, Nishida K, Itoh M, Kamimura D, Park S-J, Mizuno K, Miyazaki J, Hibi M, Ishihara K, Nakajima K, Hirano T, Tissue-Specific Autoregulation of thestat3 Gene and Its Role in Interleukin-6-Induced Survival Signals in T Cells, Mol. Cell. Biol 21, 6615–6625 (2001). [PubMed: 11533249]

39. Kwon M-J, Ma J, Ding Y, Wang R, Sun Z, Protein Kinase C-θ Promotes Th17 Differentiation via Upregulation of Stat3, J. Immunol 188, 5887–5897 (2012). [PubMed: 22586032]

40. Liu L, Okada S, Kong XF, Kreins AY, Cypowyj S, Abhyankar A, Toubiana J, Itan Y, Audry M, Nitschke P, Masson C, Toth B, Flatot J, Migaud M, Chrabieh M, Kochetkov T, Bolze A, Borghesi A, Toulon A, Hiller J, Eyerich S, Eyerich K, Gulacsy V, Chernyshova L, Chernyshov V, Bondarenko A, Grimaldo RM, Blancas-Galicia L, Beas IM, Roesler J, Magdorf K, Engelhard D, Thumerelle C, Burgel PR, Hoernes M, Drexel B, Seger R, Kusuma T, Jansson AF, Sawalle-Belohradsky J, Belohradsky B, Jouanguy E, Bustamante J, Bue M, Karin N, Wildbaum G, Bodemer C, Lortholary O, Fischer A, Blanche S, Al-Muhsen S, Reichenbach J, Kobayashi M, Rosales FE, Lozano CT, Kilic SS, Oleastro M, Etzioni A, Traidl-Hoffmann C, Renner ED, Abel L, Picard C, Marodi L, Boisson-Dupuis S, Puel A, Casanova JL, Gain-of-function human STAT1 mutations impair IL-17 immunity and underlie chronic mucocutaneous candidiasis, J. Exp. Med 208, 1635–48 (2011). [PubMed: 21727188]

41. van de Veerdonk FL, Plantinga TS, Hoischen A, Smeekens SP, Joosten LAB, Gilissen C, Arts P, Rosentul DC, Carmichael AJ, Smits-van der Graaf CAA, Kullberg BJ, van der Meer JWM, Lilic D, Veltman JA, Netea MG, STAT1 Mutations in Autosomal Dominant Chronic Mucocutaneous Candidiasis, N. Engl. J. Med 365, 54–61 (2011). [PubMed: 21714643]

42. Okada S, Markle JG, Deenick EK, Mele F, Averbuch D, Lagos M, Alzahrani M, Al-Muhsen S, Halwani R, Ma CS, Wong N, Soudais C, Henderson LA, Marzouqa H, Shamma J, Gonzalez M, Martinez-Barricarte R, Okada C, Avery DT, Latorre D, Deswarte C, Jabot-Hanin F, Torrado E, Fountain J, Belkadi A, Itan Y, Boisson B, Migaud M, Arlehamn CSL, Sette A, Breton S, McCluskey J, Rossjohn J, de Villartay J-P, Moshous D, Hambleton S, Latour S, Arkwright PD, Picard C, Lantz O, Engelhard D, Kobayashi M, Abel L, Cooper AM, Notarangelo LD, Boisson-Dupuis S, Puel A, Sallusto F, Bustamante J, Tangye SG, Casanova J-L, Impairment of immunity to Candida and Mycobacterium in humans with bi-allelic RORC mutations, Science 349, 606–613 (2015). [PubMed: 26160376]

43. Toubiana J, Okada S, Hiller J, Oleastro M, Gomez ML, Becerra JCA, Ouachée-Chardin M, Fouyssac F, Girisha KM, Etzioni A, Montfrans JV, Camcioglu Y, Kerns LA, Belohradsky B, Blanche S, Bousfiha A, Rodriguez-Gallego C, Meyts I, Kisand K, Reichenbach J, Renner ED, Rosenzweig S, Grimbacher B, van de Veerdonk FL, Traidl-Hoffmann C, Picard C, Marodi L, Morio T, Kobayashi M, Lilic D, Milner JD, Holland S, Casanova J-L, Puel A, Heterozygous STAT1 gain-of-function mutations underlie an unexpectedly broad clinical phenotype, Blood 127, 3154–3164 (2016). [PubMed: 27114460]

44. Lévy R, Okada S, Béziat V, Moriya K, Liu C, Chai LYA, Migaud M, Hauck F, Ali AA, Cyrus C, Vatte C, Patiroglu T, Unal E, Ferneiny M, Hyakuna N, Nepesov S, Oleastro M, Ikinciogullari A, Dogu F, Asano T, Ohara O, Yun L, Mina ED, Bronnimann D, Itan Y, Gothe F, Bustamante J, Boisson-Dupuis S, Tahuil N, Aytekin C, Salhi A, Muhsen SA, Kobayashi M, Toubiana J, Abel L, Li X, Camcioglu Y, Celmeli F, Klein C, AlKhater SA, Casanova J-L, Puel A, Genetic, immunological, and clinical features of patients with bacterial and fungal infections due to inherited IL-17RA deficiency, Proc. Natl. Acad. Sci 113, E8277–E8285 (2016). [PubMed: 27930337]

45. Ling Y, Cypowyj S, Aytekin C, Galicchio M, Camcioglu Y, Nepesov S, Ikinciogullari A, Dogu F, Belkadi A, Levy R, Migaud M, Boisson B, Bolze A, Itan Y, Goudin N, Cottineau J, Picard C, Abel L, Bustamante J, Casanova J-L, Puel A, Inherited IL-17RC deficiency in patients with chronic mucocutaneous candidiasis, J. Exp. Med 212, 619–631 (2015). [PubMed: 25918342]

46. Boisson B, Wang C, Pedergnana V, Wu L, Cypowyj S, Rybojad M, Belkadi A, Picard C, Abel L, Fieschi C, Puel A, Li X, Casanova J-L, An ACT1 Mutation Selectively Abolishes Interleukin-17 Responses in Humans with Chronic Mucocutaneous Candidiasis, Immunity 39, 676–686 (2013). [PubMed: 24120361]

47. de Beaucoudrey L, Puel A, Filipe-Santos O, Cobat A, Ghandil P, Chrabieh M, Feinberg J, von Bernuth H, Samarina A, Janniere L, Fieschi C, Stephan JL, Boileau C, Lyonnet S, Jondeau G, Cormier-Daire V, Le Merrer M, Hoarau C, Lebranchu Y, Lortholary O, Chandesris MO, Tron F, Gambineri E, Bianchi L, Rodriguez-Gallego C, Zitnik SE, Vasconcelos J, Guedes M, Vitor AB, Marodi L, Chapel H, Reid B, Roifman C, Nadal D, Reichenbach J, Caragol I, Garty BZ, Dogu F, Camcioglu Y, Gulle S, Sanal O, Fischer A, Abel L, Stockinger B, Picard C, Casanova JL, Mutations in STAT3 and IL12RB1 impair the development of human IL-17-producing T cells, J. Exp. Med 205, 1543–50 (2008). [PubMed: 18591412]

48. Milner JD, Brenchley JM, Laurence A, Freeman AF, Hill BJ, Elias KM, Kanno Y, Spalding C, Elloumi HZ, Paulson ML, Davis J, Hsu A, Asher AI, O'Shea J, Holland SM, Paul WE, Douek DC, Impaired TH17 cell differentiation in subjects with autosomal dominant hyper-IgE syndrome, Nature 452, 773–776 (2008). [PubMed: 18337720]

49. Acosta-Rodriguez EV, Rivino L, Geginat J, Jarrossay D, Gattorno M, Lanzavecchia A, Sallusto F, Napolitani G, Surface phenotype and antigenic specificity of human interleukin 17–producing T helper memory cells, Nat. Immunol 8, 639–646 (2007). [PubMed: 17486092]

50. Ma CS, Wong N, Rao G, Avery DT, Torpy J, Hambridge T, Bustamante J, Okada S, Stoddard JL, Deenick EK, Pelham SJ, Payne K, Boisson-Dupuis S, Puel A, Kobayashi M, Arkwright PD, Kilic SS, El Baghdadi J, Nonoyama S, Minegishi Y, Mahdaviani SA, Mansouri D, Bousfiha A, Blincoe AK, French MA, Hsu P, Campbell DE, Stormon MO, Wong M, Adelstein S, Smart JM, Fulcher DA, Cook MC, Phan TG, Stepensky P, Boztug K, Kansu A, İkincioğullari A, Baumann U, Beier R, Roscioli T, Ziegler JB, Gray P, Picard C, Grimbacher B, Warnatz K, Holland SM, Casanova J-L, Uzel G, Tangye SG, Monogenic mutations differentially affect the quantity and quality of T follicular helper cells in patients with human primary immunodeficiencies, J. Allergy Clin. Immunol 136, 993–1006.e1 (2015). [PubMed: 26162572]

51. Bønnelykke K, Sparks R, Waage J, Milner JD, Genetics of allergy and allergic sensitization: common variants, rare mutations, Curr. Opin. Immunol 36, 115–126 (2015). [PubMed: 26386198]

52. Ma CA, Stinson JR, Zhang Y, Abbott JK, Weinreich MA, Hauk PJ, P. R. Reynolds, Lyons JJ, Nelson CG, Ruffo E, Dorjbal B, Glauzy S, Yamakawa N, Arjunaraja S, Voss K, Stoddard J, Niemela J, Zhang Y, Rosenzweig SD, McElwee JJ, DiMaggio T, Matthews HF, Jones N, Stone KD, Palma A, Oleastro M, Prieto E, Bernasconi AR, Dubra G, Danielian, Zaiat J, Marti MA, Kim B, Cooper MA, Romberg N, Meffre E, Gelfand EW, Snow AL, Milner JD, Germline hypomorphic CARD11 mutations in severe atopic disease, Nat. Genet 49, 1192–1201 (2017). [PubMed: 28628108]

53. Hennino A, Vocanson M, Toussaint Y, Rodet K, Benetière J, Schmitt A-M, Aries M-F, Bérard F, Rozières A, Nicolas J-F, Skin-Infiltrating CD8+ T Cells Initiate Atopic Dermatitis Lesions, J. Immunol 178, 5571–5577 (2007). [PubMed: 17442939]

54. Hennino A, Jean-Decoster C, Giordano-Labadie F, Debeer S, Vanbervliet B, Rozières A, Schmitt A-M, Nicolas J-F, CD8+ T cells are recruited early to allergen exposure sites in atopy patch test reactions in human atopic dermatitis, J. Allergy Clin. Immunol 127, 1064–1067 (2011). [PubMed: 21236476]

55. Rosenberg HF, Dyer KD, Foster PS, Eosinophils: changing perspectives in health and disease, Nat. Rev. Immunol 13, 9–22 (2013). [PubMed: 23154224]

56. Kaplan MH, Hufford MM, Olson MR, The development and in vivo function of T helper 9 cells, Nat. Rev. Immunol 15, 295–307 (2015). [PubMed: 25848755]

57. Bocchini CE, Nahmod K, Katsonis P, Kim S, Kasembeli MM, Freeman A, Lichtarge O, Makedonas G, Tweardy DJ, Protein stabilization improves STAT3 function in autosomal dominant hyper-IgE syndrome, Blood 128, 3061–3072 (2016). [PubMed: 27799162]

58. Pelham SJ, Lenthall HC, Deenick EK, Tangye SG, Elucidating the effects of disease-causing mutations on STAT3 function in autosomal-dominant hyper-IgE syndrome, J. Allergy Clin. Immunol 138, 1210–1213.e5 (2016). [PubMed: 27315770]

59. Wienke J, Janssen W, Scholman R, Spits H, van Gijn M, Boes M, van Montfrans J, Moes N, de Roock S, A novel human STAT3 mutation presents with autoimmunity involving Th17 hyperactivation, Oncotarget 6, 20037–20042 (2015). [PubMed: 26343524]

60. Yang XO, Panopoulos AD, Nurieva R, Chang SH, Wang D, Watowich SS, Dong C, STAT3 Regulates Cytokine-mediated Generation of Inflammatory Helper T Cells, J. Biol. Chem 282, 9358–9363 (2007). [PubMed: 17277312]

61. Boisson-Dupuis S, Kong XF, Okada S, Cypowyj S, Puel A, Abel L, Casanova JL, Inborn errors of human STAT1: allelic heterogeneity governs the diversity of immunological and infectious phenotypes, Curr. Opin. Immunol 24, 364–78 (2012). [PubMed: 22651901]

62. Casanova J-L, Abel L, Quintana-Murci L, Immunology Taught by Human Genetics, Cold Spring Harb. Symp. Quant. Biol 78, 157–172 (2013). [PubMed: 24092470]

63. Notarangelo LD, Fleisher TA, Targeted strategies directed at the molecular defect: Toward precision medicine for select primary immunodeficiency disorders, J. Allergy Clin. Immunol 139, 715–723 (2017). [PubMed: 28270363]

64. Zhang Y, Su HC, Lenardo MJ, Genomics is rapidly advancing precision medicine for immunological disorders, Nat. Immunol 16, 1001–1004 (2015). [PubMed: 26382860]

65. Casanova J-L, Abel L, Human genetics of infectious diseases: Unique insights into immunological redundancy, Semin. Immunol. In press (2017), doi:10.1016/j.smim.2017.12.008.

66. Leonard WJ, O'Shea JJ, JAKS AND STATS: Biological Implications, Annu. Rev. Immunol 16, 293–322 (1998). [PubMed: 9597132]

67. Levy DE, Darnell JE, STATs: transcriptional control and biological impact, Nat. Rev. Mol. Cell Biol 3, 651–662 (2002). [PubMed: 12209125]

68. Yang J, Liao X, Agarwal MK, Barnes L, Auron PE, Stark GR, Unphosphorylated STAT3 accumulates in response to IL-6 and activates transcription by binding to NFκB, Genes Dev 21, 1396–1408 (2007). [PubMed: 17510282]

69. Villarino AV, Kanno Y, O'Shea JJ, Mechanisms and consequences of Jak-STAT signaling in the immune system, Nat. Immunol 18, 374–384 (2017). [PubMed: 28323260]

70. Flanagan SE, Haapaniemi E, Russell MA, Caswell R, Allen HL, De Franco E, McDonald TJ, Rajala H, Ramelius A, Barton J, Heiskanen K, Heiskanen-Kosma T, Kajosaari M, Murphy NP, Milenkovic T, Seppänen M, Lernmark Å, Mustjoki S, Otonkoski T, Kere J, Morgan NG, Ellard S, Hattersley AT, Activating germline mutations in STAT3 cause early-onset multi-organ autoimmune disease, Nat. Genet 46, 812–814 (2014). [PubMed: 25038750]

71. Haapaniemi EM, Kaustio M, Rajala HLM, van Adrichem AJ, Kainulainen L, Glumoff V, Doffinger R, Kuusanmäki H, Heiskanen-Kosma T, Trotta L, Chiang S, Kulmala P, Eldfors S, Katainen R, Siitonen S, Karjalainen-Lindsberg M-L, Kovanen PE, Otonkoski T, Porkka K, Heiskanen K, Hänninen A, Bryceson YT, Uusitalo-Seppälä R, Saarela J, Seppänen M, Mustjoki S, Kere J, Autoimmunity, hypogammaglobulinemia, lymphoproliferation, and mycobacterial disease in patients with activating mutations in STAT3, Blood 125, 639–648 (2015). [PubMed: 25349174]

72. Milner JD, Vogel TP, Forbes L, Ma CA, Stray-Pedersen A, Niemela JE, Lyons JJ, Engelhardt KR, Zhang Y, Topcagic N, Roberson EDO, Matthews H, Verbsky JW, Dasu T, Vargas-Hernandez A, Varghese N, McClain KL, Karam LB, Nahmod K, Makedonas G, Mace EM, Sorte HS, Perminow G, Rao VK, O'Connell MP, Price S, Su HC, Butrick M, McElwee J, Hughes JD, Willet J, Swan D, Xu Y, Santibanez-Koref M, Slowik V, Dinwiddie DL, Ciaccio CE, Saunders CJ, Septer S, Kingsmore SF, White AJ, Cant AJ, Hambleton S, Cooper MA, Early-onset lymphoproliferation and autoimmunity caused by germline STAT3 gain-of-function mutations, Blood 125, 591–599 (2015). [PubMed: 25359994]

73. Grimbacher B, Schäffer AA, Holland SM, Davis J, Gallin JI, Malech HL, Atkinson TP, Belohradsky BH, Buckley RH, Cossu F, Español T, Garty BZ, Matamoros N, Myers LA, Nelson RP, Ochs HD, Renner ED, Wellinghausen N, Puck JM, Genetic linkage of hyper-IgE syndrome to chromosome 4., Am. J. Hum. Genet 65, 735(1999). [PubMed: 10441580]

74. Li H, Durbin R, Fast and accurate long-read alignment with Burrows–Wheeler transform, Bioinformatics 26, 589–595 (2010). [PubMed: 20080505]

75. McKenna A, Hanna M, Banks E, Sivachenko A, Cibulskis K, Kernytsky A, Garimella K, Altshuler D, Gabriel S, Daly M, DePristo MA, The Genome Analysis Toolkit: A MapReduce framework for analyzing next-generation DNA sequencing data, Genome Res 20, 1297–1303 (2010). [PubMed: 20644199]

76. Li H, Handsaker B, Wysoker A, Fennell T, Ruan J, Homer N, Marth G, Abecasis G, Durbin R, The Sequence Alignment/Map format and SAMtools, Bioinformatics 25, 2078–9 (2009). [PubMed: 19505943]

77. Adzhubei IA, Schmidt S, Peshkin L, Ramensky VE, Gerasimova A, Bork P, Kondrashov AS, Sunyaev SR, A method and server for predicting damaging missense mutations, Nat. Methods 7, 248–9 (2010). [PubMed: 20354512]

78. Ng PC, Henikoff S, Predicting Deleterious Amino Acid Substitutions, Genome Res 11, 863–874 (2001). [PubMed: 11337480]

79. Fleckenstein B, Ensser A, in Current Protocols in Immunology, (John Wiley & Sons, Inc., 2001).

80. Zhang Y, Liu T, Meyer CA, Eeckhoute J, Johnson DS, Bernstein BE, Nusbaum C, Myers RM, Brown M, Li W, Liu XS, Model-based Analysis of ChIP-Seq (MACS), Genome Biol 9, R137(2008). [PubMed: 18798982]

81. McCarthy DJ, Chen Y, Smyth GK, Differential expression analysis of multifactor RNA-Seq experiments with respect to biological variation, Nucleic Acids Res 40, 4288–4297 (2012). [PubMed: 22287627]

82. Béziat V, Descours B, Parizot C, Debré P, Vieillard V, NK Cell Terminal Differentiation: Correlated Stepwise Decrease of NKG2A and Acquisition of KIRs, PLoS ONE 5, e11966(2010). [PubMed: 20700504]

83. Bjorkstrom NK, Riese P, Heuts F, Andersson S, Fauriat C, Ivarsson MA, Bjorklund AT, Flodstrom-Tullberg M, Michaelsson J, Rottenberg ME, Guzman CA, Ljunggren HG, Malmberg KJ, Expression patterns of NKG2A, KIR, and CD57 define a process of CD56dim NK-cell differentiation uncoupled from NK-cell education, Blood 116, 3853–64 (2010). [PubMed: 20696944]

84. Lim AI, Li Y, Lopez-Lastra S, Stadhouders R, Paul F, Casrouge A, Serafini N, Puel A, Bustamante J, Surace L, Masse-Ranson G, David E, Strick-Marchand H, Le Bourhis L, Cocchi R, Topazio D, Graziano P, Muscarella LA, Rogge L, Norel X, Sallenave J-M, Allez M, Graf T, Hendriks RW, Casanova J-L, Amit I, Yssel H, Di Santo JP, Systemic Human ILC Precursors Provide a Substrate for Tissue ILC Differentiation, Cell 168, 1086–1100.e10 (2017). [PubMed: 28283063]

85. de Paus RA, Geilenkirchen MA, van Riet S, van Dissel JT, van de Vosse E, Differential expression and function of human IL-12Rβ2 polymorphic variants, Mol. Immunol 56, 380–389 (2013). [PubMed: 23911393]

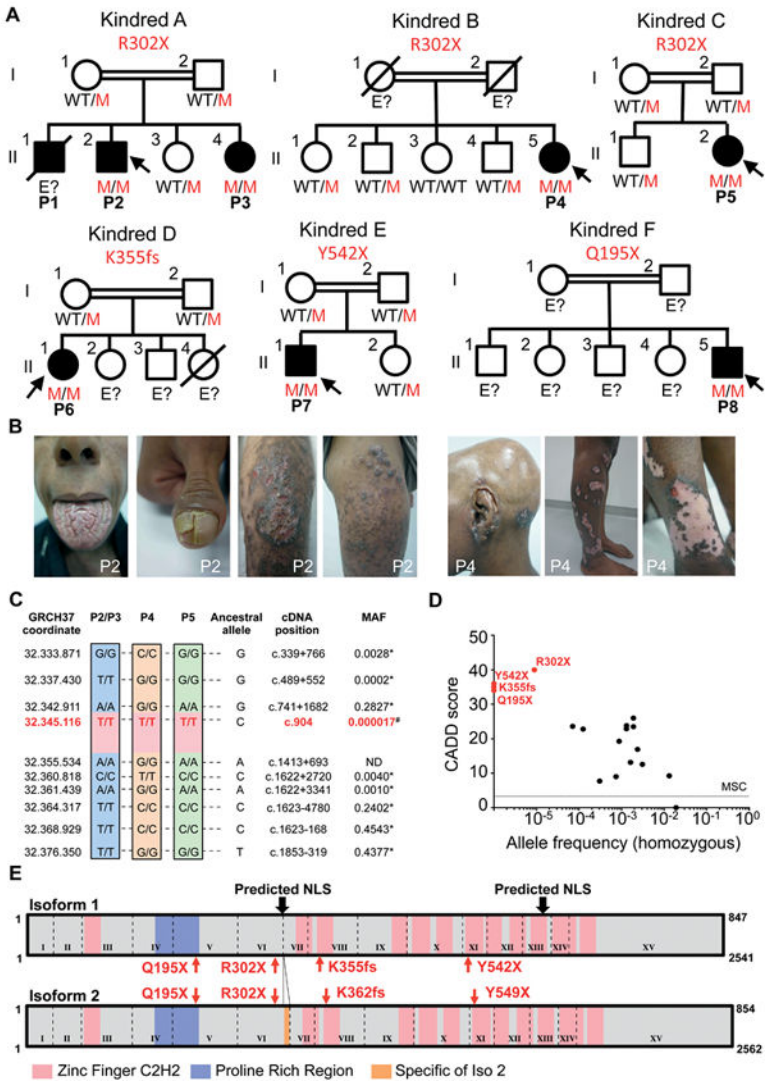

Fig. 1. Autosomal recessive *ZNF341* deficiency.

(**A**) Pedigrees of the six unrelated families, showing familial segregation of the *c.904C>T* (p.R302X) mutant *ZNF341* allele in kindreds A-C, and of alleles *c.1062delG* (p.K355fs), *c.1647C>G* (p.Y542X), and *c.583C>T* (p.Q195X) in kindreds D-F, respectively. Generations are designated by a Roman numeral (I, II). P1–P8 are represented by black symbols; the probands are indicated by arrows. Individuals of unknown genotype are labeled with "E?" (**B**) Representative images of the cutaneous phenotypes of P2 and P4, with tongue and thumb candidiasis, eczematous lesions of the thighs, with excoriated and lichenified lesions (P2), and atrophic hypopigmented scars (P4). (**C**) Comparison of the patients' haplotypes with ancestral alleles. MAF, minor allele frequency. Stars and hash tags indicate frequencies extracted from dbSNP and EXAC, respectively. (**D**) Frequency and Combined Annotation–Dependent Depletion score (CADD), for all homozygous variants reported in the ExAC database. The dotted line corresponds to the mutation significance cutoff (MSC). The CADD scores of 34, 35, 36 and 40 for the Q195X, K355fs/K362fs, Y542X/Y549X and R302X mutations, respectively, are well above the MSC of 3.31 for *ZNF341 (34)*. The

ZNF341 gene has intermediate gene damage index (GDI) and neutrality index (NI) scores, of 3.72 and 0.30, respectively, suggesting that *ZNF341* is not under strong purifying selection, consistent with the segregation of *ZNF341* deficiency as an AR disorder. (**E**) Schematic representation of the ZNF341 protein. ZNF341 has two main isoforms, isoform 1 and isoform 2, differing by 21 in-frame nucleotides at the 3' end of exon 6 of the gene, resulting in proteins of 847 and 854 amino acids in length, respectively. Exons are designated by Roman numerals. Exon boundaries are depicted with dashed lines. Predicted zinc finger domains (C2H2) and proline-rich regions are shown as light red and blue boxes, respectively. Red arrows indicate the mutations. The predicted NLS sequences are indicated with thick black arrows.

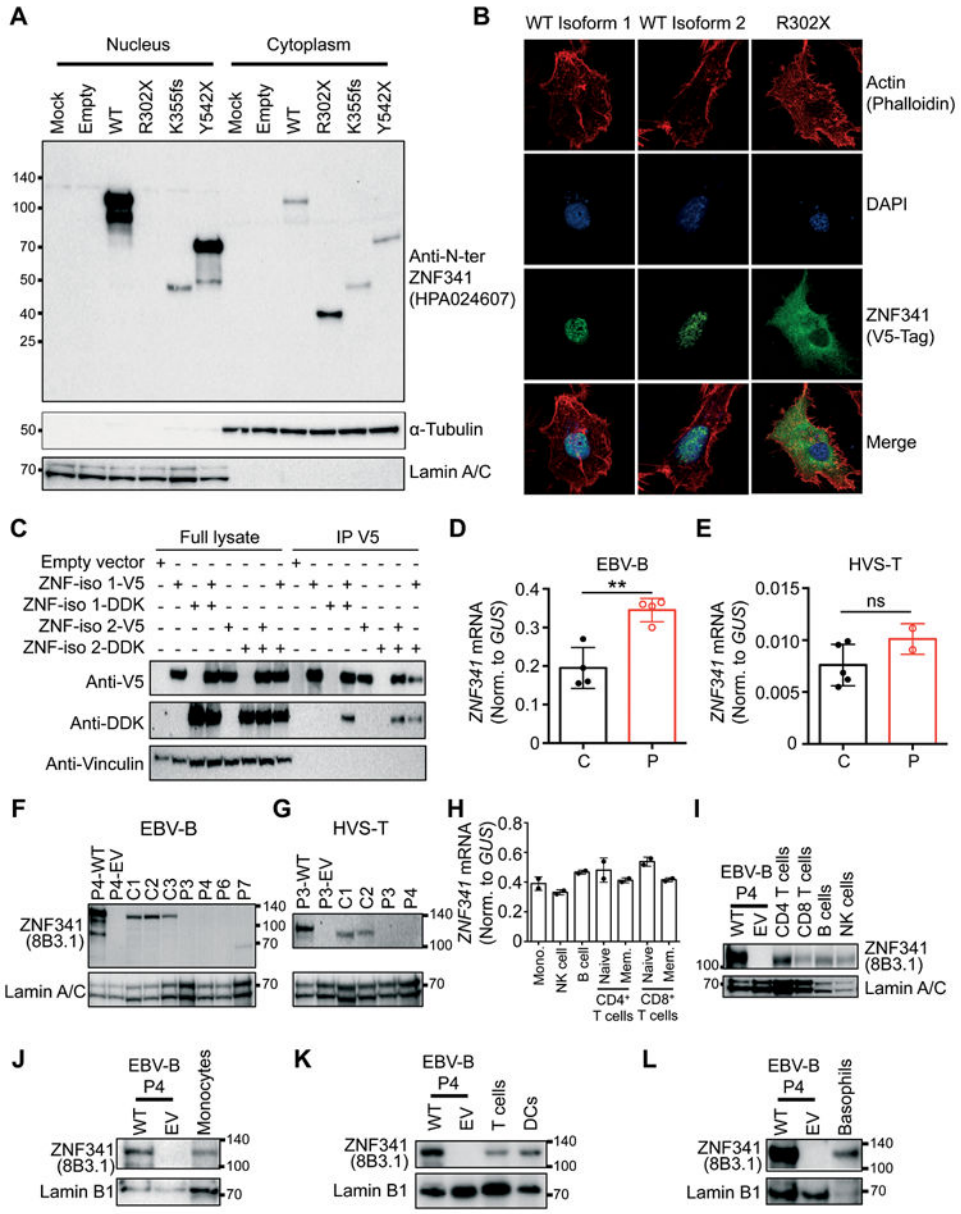

Fig. 2. Molecular characterization of *ZNF341* mutations and their expression in leukocyte subsets.

(**A**) HEK293T cells were transfected with an empty pCDNA plasmid or with pCDNA plasmids encoding the wild-type (WT), R302X, K355fs, or Y542X ZNF341 isoform 1. Cytoplasmic and nuclear fractions were separated and subjected to immunoblotting with a polyclonal Ab (pAb) against the N-terminal segment of ZNF341 (HPA024607). α-tubulin and lamin A/C were used as controls for the cytoplasmic and nuclear fractions, respectively. Western blots representative of three different experiments are shown. (**B**) SV40-fibroblasts from P4 were transfected with constructs encoding the two WT ZNF341 isoforms or the R302X mutant isoform, with a V5 tag at their C-terminus. Cells were analyzed by confocal microscopy 24 hours after transfection. WT and mutant ZNF341 isoforms were detected with an anti-V5 antibody. The cytoplasm and nucleus were identified by phalloidin and

DAPI staining, respectively. An example of staining representative of three independent experiments is shown. (**C**) HEK293T cells were cotransfected with empty plasmid or plasmids containing cDNAs encoding WT isoform 1 and/or 2 of ZNF341, each tagged C-terminally with either V5 or Myc/DDK. Whole-cell lysates (left panel) or anti-V5 immunoprecipitates (right panel) are shown. Vinculin was used as a loading control. Results representative of three independent experiments are shown. (**D-E**) RNA extracted from (D) the Epstein-Barr virus-immortalized B (EBV-B) cells of four controls and P3, P4, P6 and P7 and (E) Saimiri-transformed T (HVS-T) cells from five controls, P3 and P4, were subjected to reverse transcription-quantitative polymerase chain reaction for total *ZNF341*. Data are displayed as $2^{-\Delta Ct}$ after normalization relative to *GUS* (endogenous control) expression (ΔCt). Results representative of three independent experiments are shown. Bars represent the mean and the standard deviation. Dots represent the mean of technical duplicates. (**F-G**) Western blot of nuclear protein extracts (50 μg) obtained from (F) EBV-B cells from P4 stably transduced with an empty vector (EV) or WT *ZNF341*, three controls and four patients (P3, P4, P6, P7) and (G) HVS-T cells from P3 stably transduced with an empty vector (EV) or WT *ZNF341*, two controls and two patients (P3 and P4), with a mouse monoclonal anti-ZNF341 antibody (8B3.1, raised against ZNF341 C-terminal residues 366–468). Lamin A/C was used as a loading control. Results representative of three independent western blots are shown. (**H**) RNA was extracted from the indicated leukocyte subsets from two healthy controls and subjected to RT-qPCR for total *ZNF341*. Data are displayed as $2^{-\Delta Ct}$ after normalization relative to *GUS* (endogenous control) expression (ΔCt). Results representative of three independent experiments are shown. Bars represent the mean and the standard deviation. Dots represent the mean of technical triplicates. (**I**) Nuclear protein extracts (50 μg) were obtained from the indicated leukocyte subsets from a healthy control and subjected to western blotting with a mouse anti-ZNF341 mAb (8B3.1). Lamin A/C was used as a loading control. Results representative of three independent experiments are shown. (**J-L**) Nuclear protein extracts were obtained from monocytes (J), $CD3^+$ T cells (K), total dendritic cells (K), and basophils (L) from a healthy control, and were subjected to western blotting with the mouse anti-ZNF341 mAb (8B3.1). We used 100 μg, 50 μg and 25 μg of nuclear protein extracts in J, K and L, respectively. Lamin B1 was used as a loading control. Nuclear extracts from P4 EBV-B cells stably transduced with an empty vector (EV) or WT *ZNF341* served as negative and positive controls, respectively, for ZNF341 expression in I-L. Results representative of three independent experiments are shown.

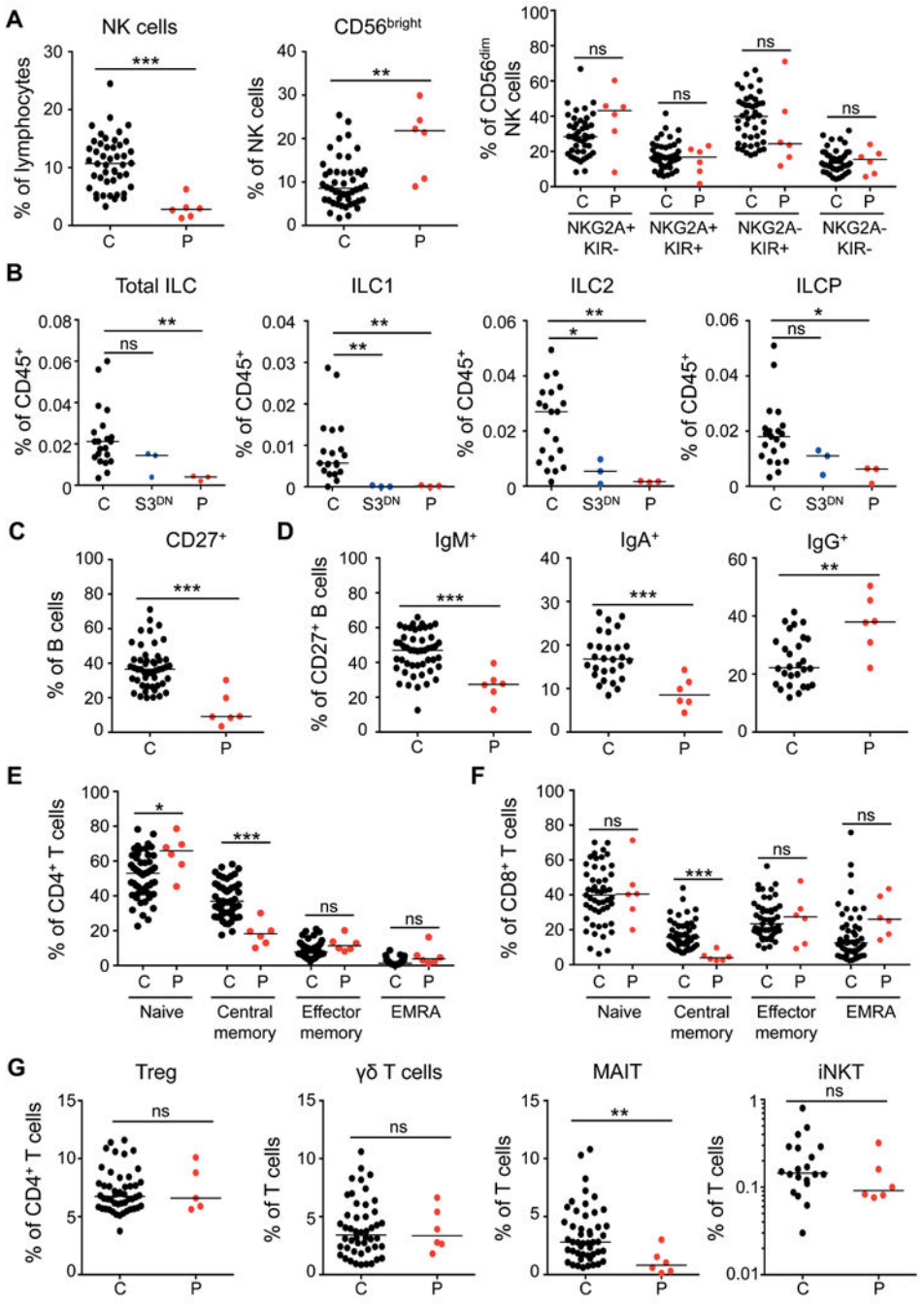

Fig. 3. NK-, ILC-, B- and T-cell subpopulation immunophenotyping.

(**A**) Natural killer cell immunophenotyping for controls (*n*=44) and patients (*n=6*, P2–P7), showing the total NK cell ($CD3^-CD56^+$) frequency in lymphocytes (left panel), the frequency of $CD56^{bright}$ cells within the NK-cell compartment (middle panel) and the terminal differentiation profile of the $CD56^{dim}$ compartment. (**B**) ILC phenotyping, showing the frequencies of total ILCs ($Lin^-CD7^+CD56^-CD127^+$), ILC1 ($EOMES^-IFN\gamma^+$), ILC2 ($GATA3^+IL13^+$) and ILCP ($CD117^+$) among the $CD45^+$ PBMCs of controls (*n*=21), ZNF341-deficient patients (*n=3*, P2–P4) and patients with *STAT3* DN mutations ($S3^{DN}$,

n=3). All analyses were conducted after the exclusion of dead cells. Mann-Whitney tests were used for comparisons. (**C**) Frequency of $CD27^+$ memory cells within the B-cell compartment of patients (*n*=6) and controls (*n*=47). Mann-Whitney tests were used for comparisons. (**D**) Frequency of IgM^+, IgA^+ and IgG^+ cells within the memory B-cell compartment of patients (*n*=6), and controls (*n*=26–47). Mann-Whitney tests were used for comparisons. (**E-F)** Frequency of naïve ($CD45RA^+CCR7^+$), central memory ($CD45RA^-CCR7^+$), effector memory ($CD45RA^-CCR7^-$) and T_{EMRA} ($CD45RA^+CCR7^-$) cells among the $CD4^+$ (E) and $CD8^+$ (F) T cells of patients (P2–P7) and controls (*n*=51). Mann-Whitney tests were used for comparisons. (**G**). T-cell subset immunophenotyping. Frequency of Treg ($CD3^+CD4^+CD25^{hi}FoxP3^+$) cells in the $CD4^+$ T-cell compartment, and frequency of γδ T cells ($CD3^+$TCR-$\gamma\delta^+$), MAIT ($CD3^+CD161^+$TCR-vα7.2^+) and iNKT ($CD3^+$TCR-$iNKT^+$) cells among the T cells of patients (*n=5* or *n=6*, P2–P7) and controls (*n*=18–46). Mann-Whitney tests were used for comparisons.

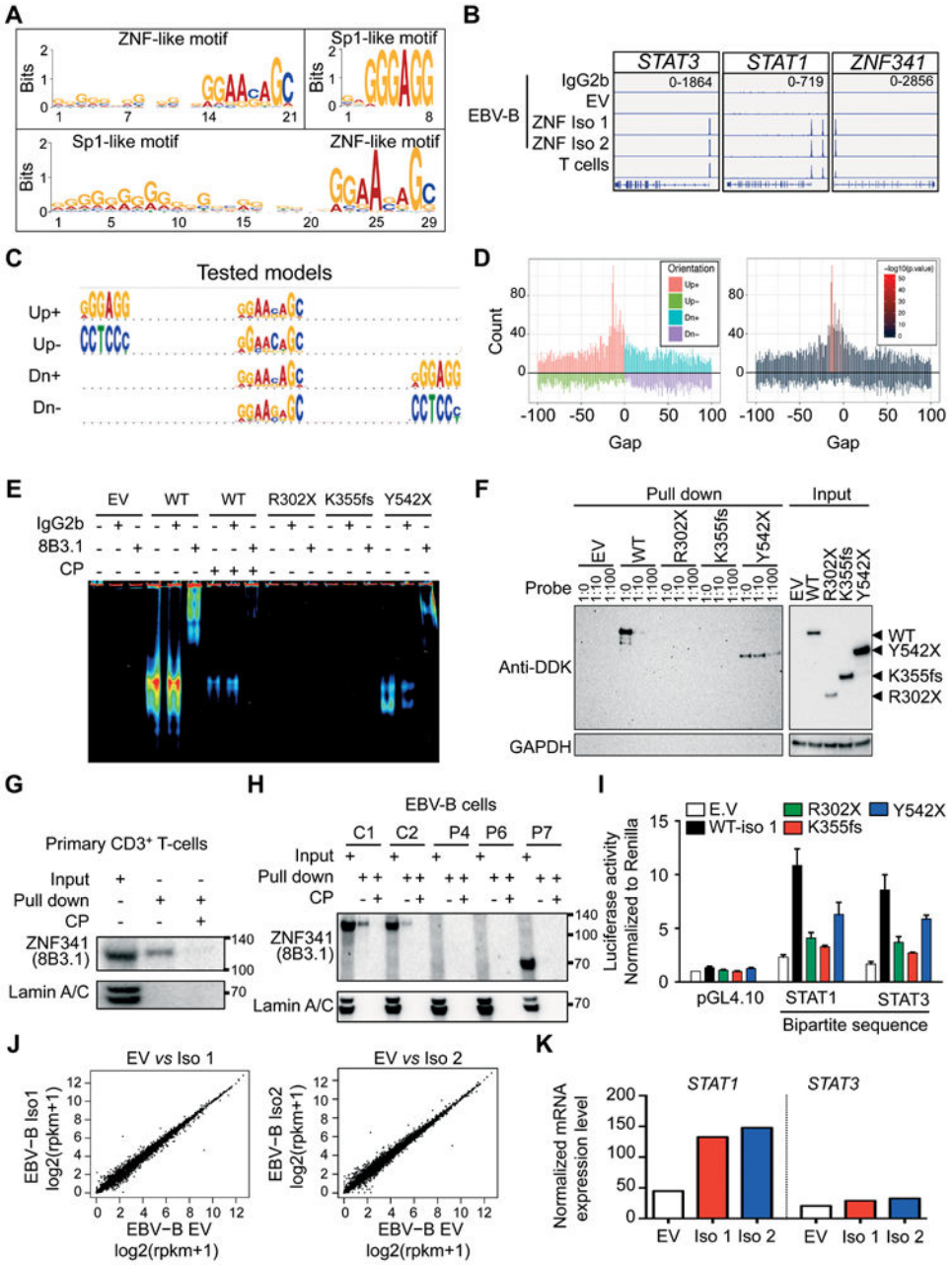

Fig. 4. Transcriptional activity of ZNF341.

(**A**) Motif analysis for the top 500 ZNF341 binding sites in P4 EBV-B cells transduced with WT *ZNF341* isoform 1, as compared with empty vector. (**B**) ChIP-Seq profile of IgG, EV, and ZNF341 (isoform 1 or isoform 2) or control $CD3^+$ T cells after 2 days of stimulation with plate-bound anti-CD3 and soluble anti-CD28 mAb for the genomic loci corresponding to *STAT3*, *STAT1* and *ZNF341*. The scale of the *y*-axis, corresponding to the number of reads, is indicated at the top right corner of each plot. **(C)** Models tested to determine the orientation and spacing preferences of the ZNF-like core motif and the Sp1-like motif. (**D**) Distribution of the observed spacing counts between the Sp1-like motif and the ZNF-like

core motif in EBV-B cells from P4 stably transduced with WT *ZNF341*. Counts are displayed relative to the model tested (left) and *p*-values are calculated for a given spacing (right). (**E**) Electrophoretic mobility shift assay (EMSA) of nuclear extracts of HEK293T cells transfected with an empty vector (EV), the C-terminal DDK-tagged WT, R302X, K355fs, or Y542X *ZNF341* alleles. Extracts were incubated with a 5' fluorescent DNA probe containing the putative bipartite ZNF341-binding motif from the *STAT3* promoter in the presence or absence of a control isotype (IgG2b) or an anti-ZNF341 mAb (8B3.1) for supershift experiments. An untagged competitor probe (CP) of similar sequence but with a concentration ten times higher was used to test binding specificity. Results representative of three independent experiments are shown. (**F**) Pulldown of the 5' biotinylated DNA probe containing the putative bipartite ZNF341-binding motif from the *STAT3* promoter after incubation with nuclear extracts of HEK293T cells transfected with an empty vector (EV), the C-terminal DDK-tagged WT, R302X, K355fs, or Y542X *ZNF341* alleles. Extracts were incubated in the presence or absence of various doses of a competitor probe (CP) to test binding specificity (1:0, 1:10 and 1:100 are the ratios of specific biotinylated probe to CP). The presence or absence of ZNF341 constructs in the pulldown fraction (left panel), or in the input (right panel) was assessed by immunoblotting for the C-terminal DDK tag. Results representative of three independent experiments are shown. (**G-H**) Pulldown of the 5' biotinylated DNA probe containing the putative bipartite ZNF341-binding motif from the *STAT3* promoter after incubation with nuclear extracts of negatively sorted primary $CD3^+$ T cells of one control (G) or of EBV-B cell lines from two controls, P4, P6 and P7 (H). Extracts were incubated in the presence or absence of a competitor probe (CP) at a concentration ten times higher than that of the biotinylated DNA probe, to test binding specificity. The presence or absence of ZNF341 in the pulldown fraction was assessed by immunoblotting with an anti-ZNF341 mAb (8B3.1). Lamin A/C was used as a loading control. Results representative of three independent experiments are shown. (**I**) Luciferase activity of HEK293T cells cotransfected with WT or mutant *ZNF341* isoform 1, plus a pGL4.10 reporter plasmid encoding the luciferase cDNA downstream from the bipartite ZNF341 binding motif of the promoters of *STAT1* and *STAT3*. The results shown are the mean and standard deviation of three independent experiments. (**J**) Total RNA sequencing data for the EBV-B cells of P4 stably transduced with WT *ZNF341* isoform 1 (Iso 1), isoform 2 (Iso 2) or an empty vector (EV). Scatter dot plots comparing mRNA levels in cells transduced with *ZNF341* isoform 1 or 2 with those in cells transduced with the empty vector. (**K**) *STAT1* and *STAT3* mRNA levels extracted from total RNA sequencing data.

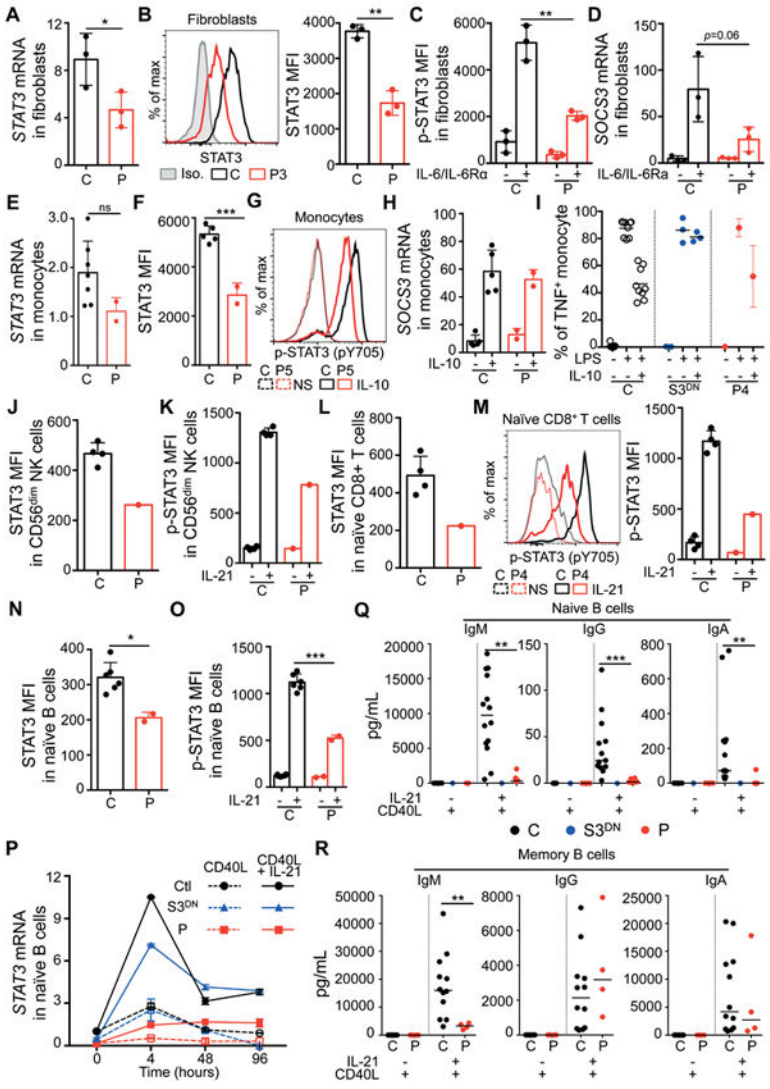

Fig. 5: STAT3 production and function in primary cells.

(A-D) STAT3 production and function in primary fibroblasts. *STAT3* mRNA levels (**A**) as evaluated by RT-qPCR after RNA extraction from the primary fibroblasts of three controls and three patients (P2–P4). Data are displayed as $2^{-\Delta Ct}$ after normalization relative to *GUS* (endogenous control) expression (ΔCt). Data representative of two independent experiments are shown. (**B**) STAT3 levels, as evaluated by flow cytometry, in primary fibroblasts. Left panel, representative image of STAT3 expression in fibroblasts from P3 and a healthy control, as well as the isotypic control. Right panel, recapitulative graph showing the mean fluorescence intensity (MFI) of STAT3, as measured by flow cytometry, in three controls, and three patients (P2–P4). Data representative of two independent experiments are shown. (**C**) Recapitulative graph of the mean fluorescence intensity (MFI) of pY705-STAT3, as evaluated by flow cytometry, in primary fibroblasts from three controls, and three patients (P2–P4), left unstimulated or after 30 minutes of stimulation with IL6/IL-6Rα. (**D**) *SOCS3* mRNA levels, as evaluated by RT-qPCR after RNA extraction from the primary fibroblasts of three controls and three patients (P2–P4), with or without two hours of stimulation with

IL6/IL-6Rα. Data are displayed as $2^{-\Delta Ct}$ after normalization relative to *GUS* (endogenous control) expression (ΔCt). Data representative of two independent experiments are shown. **(E-I)** STAT3 production and function in monocytes. *STAT3* mRNA levels (E), as evaluated by RT-qPCR after RNA extraction from the primary monocytes of three controls, P4 and P5. Data are displayed as $2^{-\Delta Ct}$ after normalization relative to *GUS* (endogenous control) expression (ΔCt). (F) STAT3 expression, as measured by flow cytometry in primary monocytes. Recapitulative graph of the mean fluorescence intensity (MFI) of STAT3, as measured by flow cytometry, in three controls, P4 and P5. (G) STAT3 phosphorylation (pY705), evaluated by flow cytometry, in monocytes from P5 and a healthy control, after 30 minutes of stimulation with IL-10. Representative image for two patients tested. (H) *SOCS3* mRNA levels, as evaluated by RT-qPCR after RNA extraction from the primary monocytes of five controls and two patients (P4 and P5), with or without two hours of stimulation with IL-10. Data are displayed as $2^{-\Delta Ct}$ after normalization relative to *GUS* (endogenous control) expression (ΔCt). (I) Percentage of TNF^{+} monocytes for nine controls, P4 (tested twice) and three STAT3-DN patients, after four hours of stimulation with LPS in the presence or absence of IL-10, as evaluated by flow cytometry. (**J**) Flow cytometry quantification of STAT3 levels in primary NK cells. Recapitulative graph of the mean fluorescence intensity (MFI) of STAT3 measured in four controls and P4. (**K**) Graph of the mean fluorescence intensity (MFI) of pY705-STAT3, as evaluated by flow cytometry, in primary $CD56^{dim}$ NK cells from four controls and P4, left unstimulated or after 30 minutes of stimulation with IL-21. (**L**) Graph of the mean fluorescence intensity (MFI) of STAT3 in primary naïve $CD8^{+}$ T cells, measured in four controls and P4. (**M**) Representation of the phosphorylation of STAT3 (pY705) in primary naïve $CD8^{+}$ T cells from one control and P4, evaluated by flow cytometry, without stimulation or after 30 minutes of stimulation with IL-21 (left panel). Right panel: graph of the mean fluorescence intensity (MFI) of pY705-STAT3, as evaluated by flow cytometry, in primary naïve $CD8^{+}$ T cells from four controls and P4, left unstimulated or after 20 minutes of stimulation with IL-21. (J-M) Data are representative of two independent experiments (P4 and P8). (**N**) Flow cytometry quantification of STAT3 levels in primary B cells. Recapitulative graph of the mean fluorescence intensity (MFI) of STAT3, as measured by flow cytometry, in six controls, P4 and P6. (**O**) Quantification of the phosphorylation of STAT3 (pY705) in primary B cells from three controls, P4 and P6, evaluated by flow cytometry, with the cells left unstimulated or after 30 minutes of stimulation with IL-21. (**P**) Levels of *STAT3* mRNA in naïve B cells from one healthy individual, one STAT3 DN patient and one ZNF341 deficient patient (P8) after 0, 4, 48 and 96 hours of stimulation with the indicated combinations of CD40L and IL-21. Data are displayed as $2^{-\Delta\Delta Ct}$ after normalization relative to *GUS* (endogenous control) expression (ΔCt) and non-stimulated cells of the control (ΔΔCt). (**Q**) Sorted naïve B cells from controls (n=14), one STAT3-DN patient, and six ZNF341 deficient patients (P2–P4, P6, P7 and P8) were cultured in the presence of CD40L (200 ng/mL), with or without IL-21 (50 ng/mL) for 7 days. The production (pg/ml) of IgM, IgG and IgA was then assessed by Ig heavy chain-specific ELISA on cell culture supernatants. (**R**) Sorted memory B cells from controls (n=12) and five ZNF341 deficient patients (P2–P4, P6 and P7) were cultured in the presence of CD40L (200 ng/mL), with or without IL-21 (50 ng/mL), for 7 days. The production (pg/ml) of IgM, IgG and IgA was then assessed by Ig heavy chain-specific ELISA on cell culture supernatants.

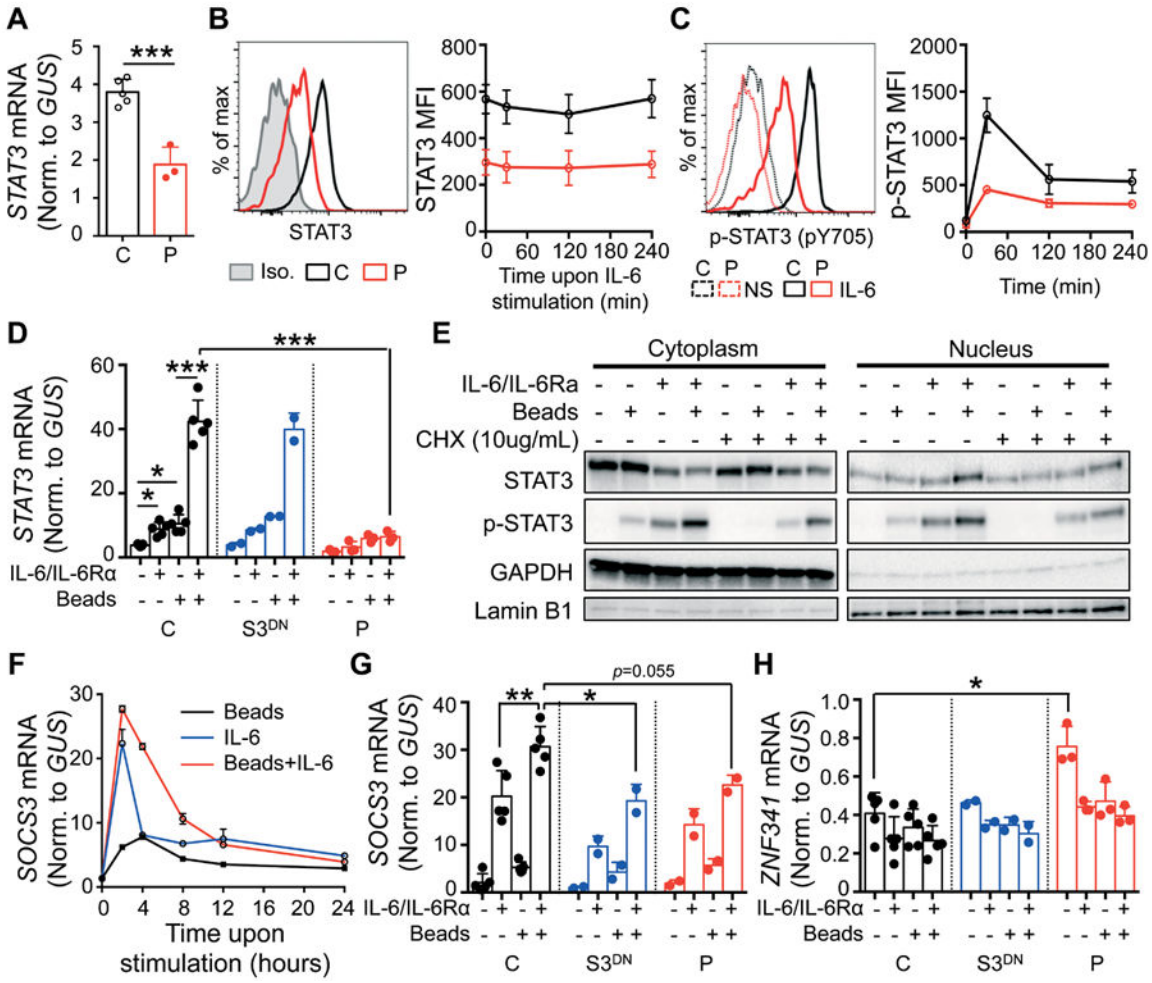

Fig. 6. Impaired STAT3 production and function in naïve CD4$^+$ cells from ZNF341-deficient patients.

(**A**) *STAT3* mRNA levels, as evaluated by RT-qPCR after RNA extraction from the naïve CD4$^+$ T cells of five controls, P4, P5 and P7. Data are displayed as $2^{-\Delta Ct}$ after normalization relative to *GUS* (endogenous control) expression (ΔCt). (**B**) STAT3 protein levels, as evaluated by flow cytometry, in naïve CD4$^+$ T cells. Left panel, representative histogram of STAT3 levels in P4, one healthy control and the isotypic control. Right panel, recapitulative graph of the mean fluorescence intensity (MFI) of STAT3, as evaluated by flow cytometry, in naïve primary CD4$^+$ T cells from five controls, P2, P3 and P4, left unstimulated or after 30, 120 and 240 minutes of stimulation with IL-6/IL-6Rα. (**C**) Flow cytometry quantification of the phosphorylation of STAT3 (pY705) in naïve CD4$^+$ T cells after stimulation with IL-6/IL-6Rα. The left panel shows a representative flow cytometry histogram for STAT3 (pY705) in the naïve CD4$^+$ T cells of P4 and in those of one healthy control, left unstimulated or after 30 minutes of stimulation with IL-6/IL-6Rα. The right panel shows a recapitulative graph of the mean fluorescence intensity (MFI) of STAT3 (pY705) for five controls, P2, P3 and P4, after 0, 30, 120 and 240 minutes of IL-6/IL-6Rα stimulation. Dots and error bars show the means and standard deviations, respectively. (**D**)

Levels of *STAT3* mRNA in thawed naïve $CD4^+$ T cells from healthy individuals (n=5), two STAT3 DN ($S3^{DN}$) patients and three ZNF341-deficient patients (P4, P5 and P7), after two hours of stimulation with the indicated combinations of IL-6/IL-6Rα and beads (anti-CD2/CD3/CD28 mAb-coated beads). Data are displayed as $2^{-\Delta Ct}$ after normalization relative to *GUS* (endogenous control) expression (ΔCt). (**E**) Western blot of cytoplasmic and nuclear protein extracts of naïve $CD4^+$ T cells obtained from one healthy control after four hours of stimulation with the indicated combinations of IL-6/IL-6Rα and beads (anti-CD2/CD3/CD28 mAb-coated beads) in the presence or absence of 10 μg/mL cycloheximide. GAPDH and lamin B1 were used as loading controls for the cytoplasmic and nuclear fractions, respectively. Data representative of three independent experiments are shown. (**F**) Induction of *SOCS3* mRNA in control naïve $CD4^+$ T cells after stimulation with IL-6/IL-6Rα and/or beads (anti-CD2/CD3/CD28 mAb-coated beads) for 0, 2, 4, 8, 12 and 24 hours. Data are displayed as $2^{-\Delta Ct}$ after normalization relative to *GUS* (endogenous control) expression (ΔCt). Dots and error bars represent the mean and standard deviation for two donors. (**G-H**) Levels of *SOCS3* (G) or *ZNF341* (H) mRNA in thawed naïve $CD4^+$ T cells from healthy individuals (n=5), two STAT3 DN patients ($S3^{DN}$) and two (P4 and P7) or three (P4, P5 and P7) ZNF341-deficient patients after two hours of stimulation with the indicated combinations of IL-6/IL-6Rα and beads (anti-CD2/CD3/CD28 mAb-coated beads). Data are displayed as $2^{-\Delta Ct}$ after normalization relative to *GUS* (endogenous control) expression (ΔCt). Bar graphs and error bars represent the mean and standard deviation.

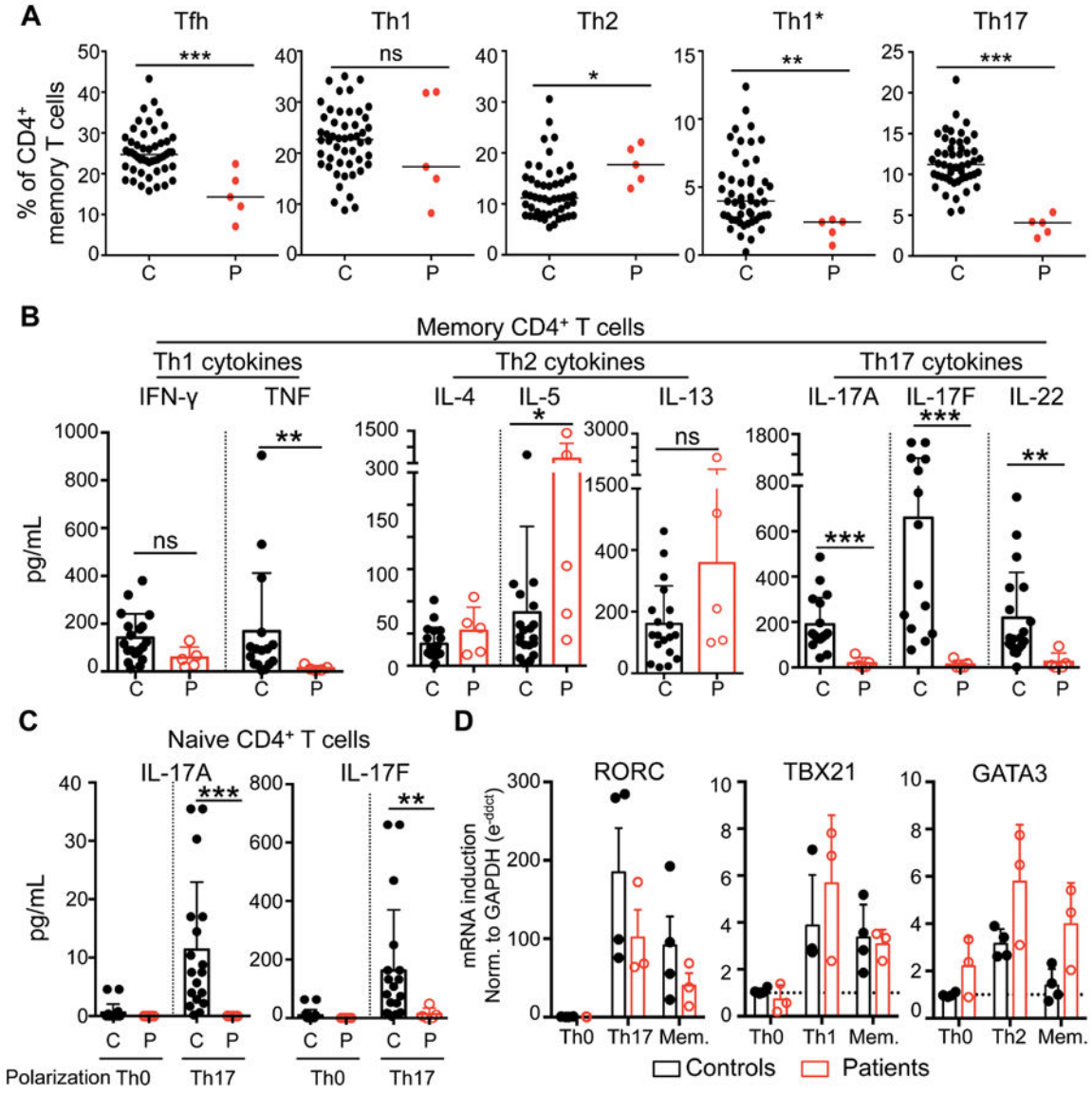

Fig. 7. Impaired Th17 differentiation in ZNF341-deficient patients.

(**A**) Frequency of T-helper (Th) subsets within the CD4$^+$ memory compartments of controls (n=49) and patients (n=5). Subsets were defined as follows: Tfh (CXCR5$^+$), Th1 (CXCR5$^-$CXCR3$^+$CCR4$^-$CCR6$^-$), Th2 (CXCR5$^-$CXCR3$^-$CCR4$^+$CCR6$^-$), Th1* (CXCR5$^-$CXCR3$^+$CCR4$^-$CCR6$^+$) and Th17 (CXCR5$^-$CXCR3$^-$CCR4$^+$CCR6$^+$). Mann-Whitney tests were used for comparisons. (**B**) Secretion (pg/ml) of Th1 (IFN-γ, TNF), Th2 (IL-4, IL-5, IL-13) and Th17 (IL-17A, IL-17F, IL-22) cytokines by memory CD4$^+$ T cells after five days of culture under Th0 conditions (anti-CD2/CD3/CD28 mAb-coated beads). Mann-Whitney tests were used for comparisons. (**C**) Secretion (pg/ml) of Th17 (IL-17A, IL-17F) cytokines by naïve CD4$^+$ T cells after five days of culture under Th0 (anti-CD2/CD3/CD28 mAb-coated beads) or Th17 (anti-CD2/CD3/CD28 mAb-coated beads together with IL-1β, IL-6, IL-21, IL-23 and TGF-β) polarizing conditions. Mann-Whitney tests were used for comparisons. (**D**) Expression of *RORC*, *TBX21* and *GATA3* by naïve CD4$^+$ T cells after five

days of culture under Th0, Th17 or Th1 (anti-CD2/CD3/CD28 mAb-coated beads together with IL-12) or Th2 (anti-CD2/CD3/CD28 antibody-coated beads together with IL-4) polarizing conditions, or by memory (Mem.) $CD4^+$ T cells, as determined by RT-qPCR, relative to *GAPDH*. Results are shown for four controls and three ZNF341-deficient patients (P2–P4).